Fluorescence and Adaptation in Color Images

by

Chi Zhang

A thesis
presented to the University of Waterloo
in fulfillment of the
thesis requirement for the degree of
Master of Mathematics
in
Computer Science

Waterloo, Ontario, Canada, 2011

I hereby declare that I am the sole author of this thesis. This is a true copy of the thesis, including any required final revisions, as accepted by my examiners.

I understand that my thesis may be made electronically available to the public.

Abstract

Color plays a vitally important role in the world we live in. It surrounds us everywhere we go. Achromatic life, restricted to black, white and grey, is extremely dull. Color fascinates artists, for it adds enormously to aesthetic appreciation, directly invoking thoughts, emotions and feelings. Color fascinates scientists. For decades, scientists in color imaging, printing and digital photography have striven to satisfy increasing demands for accuracy in color reproduction.

Fluorescence is a very common phenomenon observed in many objects such as gems and corals, writing paper, clothes, and even laundry detergent. Traditional color imaging algorithms exclude fluorescence by assuming that all objects have only an ordinary reflective component. The first part of the thesis shows that the color appearance of an object with both reflective and fluorescent components can be represented as a linear combination of the two components. A linear model allows us to separate the two components using independent component analysis (ICA). We can then apply different algorithms to each component, and combine the results to form images with more accurate color.

Displaying color images accurately is as important as reproducing color images accurately. The second part of the thesis presents a new, practical model for displaying color images on self-luminous displays such as LCD monitors. It shows that the model accounts for human visual system's mixed adaptation condition and produces results comparable to many existing algorithms.

Acknowledgements

I would like to express my appreciation to all the people in my life who have been giving me unconditional love and support. I would like to extend special thanks to my supervisor Professor Bill Cowan, for his guidance, enthusiasm, support and patience. Special thanks to my supervisor Professor Imari Sato, at National Institute of Informatics (NII) in Japan, for generously offering her ideas and support. Without her, none of the nice images on fluorescence would exist. To my readers Professor Stephen Mann and Professor Jeff Orchard, thank you for your time, support, and valuable opinions.

Thanks to all CGL members, for the icecream on Tuesdays, weekly coffee hours, almost-monthly potlucks, morning espresso, daily jokes (especially from Craig), and the re-arrangement of my desk. Thank you Elodie for being there for me when I was about to go crazy.

Thanks to all my other friends (VL, RC, DK, YZ, DL, JW, HT...), especially Chloe and Claire, for always being there for me.

I owe deepest gratitude to my parents, for everything they have done for me.

On a personal note, I would like to thank KW. Thank you for your understanding and encouragement three years ago. Without you, I would not have been here. Also, I owe you deepest apologies.

Dedication

To my dearest parents, for their unconditional love, understanding, and support.

Table of Contents

List of Tables

List of Figures

Chapter 1

Introduction

Color plays a vitally important role in the world we live in. It surrounds us everywhere we go. Achromatic life with only black, white and grey would be extremely dull. Color fascinates artists, for it adds enormously to aesthetic appreciation. Artists manipulate color in their design to provoke thoughts, convey emotions and induce feelings. Color also fascinates scientists. For decades, scientists in color imaging, printing and digital photography have striven to satisfy increasing demands for accuracy in color reproduction. As a researcher in computer graphics, my goal is to explore how to reproduce the color of objects realistically on computer displays. To achieve such a goal, two questions must be considered: how to reproduce color accurately and how to display color accurately.

Fluorescence in color imaging

For decades, researchers in computational color constancy have proposed many algorithms and models to predict the true color of objects in images [2, 16, 10]. Researchers in image reproduction and realistic rendering strive to reproduce objects with accurate color under arbitrary illumination conditions [23, 41]. While algorithms for computing color appearance vary greatly, they share a common assumption: none of the objects in the scene exhibit fluorescence. Fluorescence is the emission of visible light by objects that are exposed to a source light covering the ultraviolet range (*e.g.* sunlight and ultraviolet light). In reality, fluorescence is a common

Figure 1.1: Fluorescent objects: gems and corals, clothes, banana and fluorescent sheets.

phenomenon observed in many objects, from gems and corals, to different kinds of writing paper and our clothes (Figure 1.1). Therefore, to handle color accurately, computer vision and image synthesis algorithms ought to take fluorescence into account.

By experimentation, I discovered that a composite object with both ordinary reflective and fluorescent components has the color appearance that is the sum of the two components interacting with illumination differently. To handle the two components correctly, it is necessary to separate them. This motivated me to develop a method for separating fluorescence from reflectance. Then assume in an ordinary color camera, the color of a generic pixel p_c on the captured image is a linear contribution

$$p_c = a_c p_{c,O} + b_c p_{c,F},$$

where $c = \{R, G, B\}$, $p_{c,O}$ and $p_{c,F}$ are the color of the ordinary reflective and fluorescent components. Let a_c and b_c be the coefficients to represent the amount of contribution from each component to the pixel color p_c. a_c and b_c depend on the interactions between each component and the illuminant[1]. Since we do not know the illumination condition under which p_c is taken, we need to solve for $p_{c,O}$ and $p_{c,F}$ when only the pixel colors, p_c, are known. To make this hard problem solvable, I assume that the reflective and fluorescent components of an image are statistically independent. The assumption is reasonable because, in the absence of image interpretation, the spatial distribution of fluorescent component is uncorrelated with the spatial distribution of the reflective component. Based on the linear contribution model, I show that given the complete set of pixels $\{p_c\}$ for two images taken under different illuminants, $p_{c,O}$ and $p_{c,F}$ can be effectively recovered using independent component analysis (ICA).

This thesis describes an attempt at separating the reflective and fluorescent components of an image. It makes the following contributions in the area of realistic color imaging:

- providing a theory of fluorescent phenomenon,
- showing that the color of a fluorescent surface is not affected by the color of its illuminant, in which it differs from an ordinary reflective surface, and

[1]The light source that illuminates the object.

- proposing a method for separating the reflective and fluorescent components of an image using ICA, and an improved method for relighting images under an arbitrary illuminant.

Display color accurately

When we view images on a self-luminous display such as an LCD monitor, our perception of color depends partly on sources of illumination portrayed by the scene, and partly on sources of illumination in the viewing environment. When the viewing environment changes, our perception of color changes, causing an undesirable discrepancy in our viewing experience. To solve such problems, color appearance models have been created to predict how perception changes with the viewing environment. These models aim to provide viewers with a viewing experience independent of illumination. The display industry now provides adaptive displays that use color appearance models to compensate for achromatic changes in the viewing environment. However, existing full-blown color appearance models have the complexity that is more than needed to support adaptive displays. In this thesis, I propose a simple model for adaptive displays based on the von Kries hypothesis, a fundamental theory for human color vision. It takes into account the chromatic adaptation mechanism that occurs in addition to achromatic adaptation when viewers look at images on displays. Compared to existing color appearance models, my model is more efficient and suitable for adaptive displays. My contributions to the science of adaptive displays are:

- proposing a practical model for adaptive displays based on the von Kries hypothesis,
- showing that the model accounts for chromatic adaptation to the illumination condition in the image and to the viewing environment,
- showing that the model is simpler than other existing full-blown color appearance models, yet produces comparable results.

The rest of the thesis is structured as follows. Chapter 2 summarizes research in spectral rendering of fluorescent objects, color perception, and adaptive displays. Chapter 3 presents a theory and experimental results on how fluorescent surfaces interact with their illuminants,

and a method for separating the ordinary reflective and fluorescent components of an image. Chapter 4 presents the derivation of my color appearance model for adaptive displays. The results, including image separation, relighting, and evaluations of the proposed color appearance model are presented in Chapter 5. Contributions, limitations and future directions of my research are discussed in Chapter 6.

Chapter 2

Related Work

The importance of reproducing color accurately and faithfully is apparent in many areas of computer science. In computer graphics, the color of illuminated objects must be rendered accurately. Computer vision and color imaging use the color appearance of objects under the current illumination to identify objects, and to predict their appearance under other illumination conditions. This chapter starts by summarizing previous research in spectral rendering of fluorescent objects.

2.1 Spectral Rendering and Fluorescence

Achieving realism is an important goal of rendering. Faithful reproduction of the color of objects compared to their real-world counterparts is an important determinant of realism. The perceived color of an object is determined by the spectral composition of the light leaving it. The makeup of this light is a combination of the *illuminant* (the light source that illuminates the object), and the object's *reflectance* (the way the object modifies the illuminant). Most common rendering techniques and platforms such as basic raytracing, OpenGL [31] and RenderMan [42] parametrize the perceived color by only three numbers, each conceived as the excitation of an RGB channel. In other words, the illuminant and reflectance are approximated by three

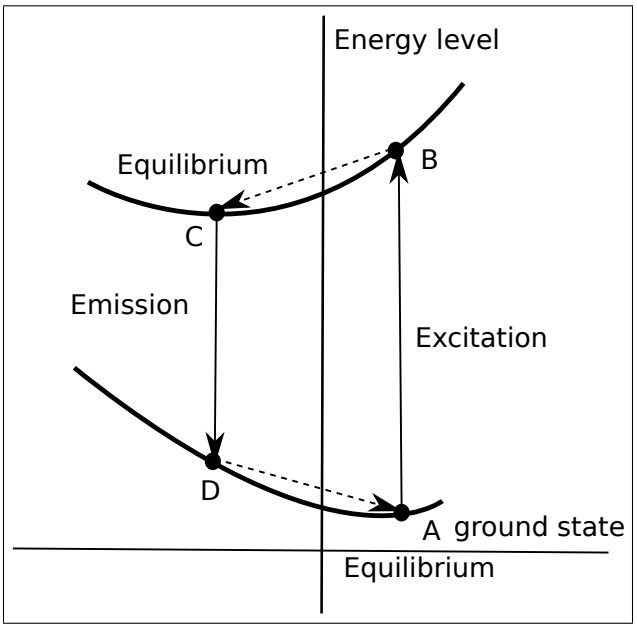

Figure 2.1: Energy-level diagram illustrating fluorescence.

color channels. To improve accuracy, researchers have often proposed *spectral rendering*, which parametrizes color by a discrete spectrum, the energy density at each of many wavelengths in the visible spectrum. A non-fluorescent object absorbs photons in the visible range, 380 nm to 720 nm. The electrons in the molecules are excited to a higher energy level but immediately drop back to the original energy state, releasing energy in the form of emitting a photon of *equal* wavelength. Therefore, for a non-fluorescent object, we specify its reflectance corresponding to each wavelength of the illuminant. The observed spectrum $\Phi(\lambda)$ of a non-fluorescent object is

$$\Phi(\lambda) \quad = \quad I(\lambda)R(\lambda), \tag{2.1}$$

where $I(\lambda)$ is the spectrum of the illuminant and $R(\lambda)$ is the reflectance of the object.

Fluorescent objects interact with illuminants differently than non-fluorescent objects. Most fluorescent objects absorb light in the near ultraviolet (UV) range, 200 nm to 380 nm, and re-emit visible light 380 nm to 720 nm. A few objects absorb short-wavelength visible light, 380 nm to 500 nm, and re-emit longer-wavelength visible light. The difference is explained by theories in

molecular physics [27] (Figure 2.1). Initially, the molecules of a fluorescent object are structured as a lattice in equilibrium in the ground energy state A. When the lattice is irradiated with incident light, the electrons are excited from the ground state A to a higher energy state B. After the transition, a re-arrangement of the ions in the lattice takes place and the system assumes an equilibrium state C. Some energy is dissipated within the lattice during the transition from B to C. From the equilibrium state C, light is emitted when electrons drop back to the ground state D. From D, the structure of the lattice is re-arranged again to reach the stable equilibrium ground state A. The lifetime of the excitation from state A to state B is 10^5 times longer than the period of lattice re-arrangement (B to C). Thus no matter how the electrons reach the excited state B, the system comes to an equilibrium state (C) before emission. This implies that the intensity of the emitted spectra of a fluorescent object depends on the incident light, but the frequency distribution does not. The *excitation spectrum* of a fluorescent object shows how much energy from the illuminant is absorbed at each wavelength; it is a function of the wavelength of the illuminant. For each wavelength in an excitation spectrum, there is a corresponding *emission spectrum* that shows the frequency distribution and intensity of the emitted light. Usually the emission spectrum is a function of wavelength covering the visible range. The frequency distribution of all emission spectra is constant, but the intensity varies. The properties of fluorescent objects are well shown with experimental results. Figure 2.2(a) shows the measured emission spectra of a red-orange fluorescent sheet. Each colored spectrum corresponds to the illuminant at different wavelength, and have the same frequency distribution as one another. Figure 2.2(b) shows the normalized [1] excitation (dotted line) and emission (solid line) spectra of the sheet. From the emission spectrum we can see that the sheet appears reddish orange when it is illuminated by light in the range of 380 nm to 650 nm.

Based on the molecular physics of fluorescent objects, researchers in computer graphics developed algorithms for rendering fluorescent objects [41, 23]. To obtain the observed spectrum of a pure fluorescent surface, we must consider the overall contribution from its illuminant, excitation and emission. Suppose the illuminant is I and its intensity at wavelength λ_i is $I(\lambda_i)$.

[1] Spectral power distribution is normalized so that the minimum intensity is 0 and the maximum intensity is 1.0.

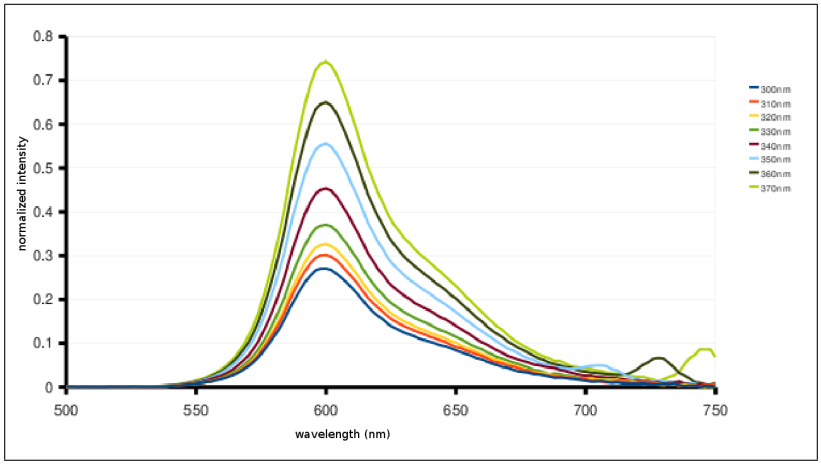

(a) Measured emission spectra of a red-orange fluorescent sheet. Each colored spectrum corresponds to the illuminant at a particular wavelength.

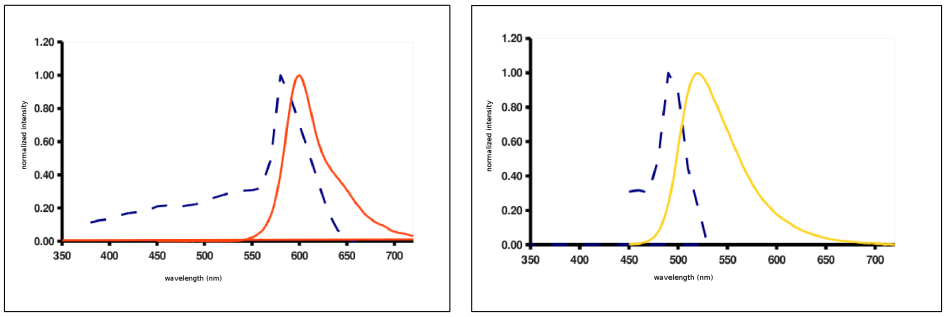

(b) Normalized excitation (dotted line) and emission (solid line) spectra of a red-orange and green-yellow fluorescent sheet.

Figure 2.2: Measured spectra of a red-orange and green-yellow fluorescent sheet.

Let K and J represent the normalized excitation and emission spectrum, respectively. Then the observed spectrum, $\Phi(\lambda, \lambda_i)$, resulting from the illuminant at λ_i is

$$\Phi(\lambda, \lambda_i) \quad = \quad I(\lambda_i)K'(\lambda_i)J(\lambda), \tag{2.2}$$

where $K'(\lambda_i) \equiv \frac{K(\lambda_i)}{\int K(\lambda_i)\,\mathrm{d}\lambda_i}$ is the relative intensity of the excitation caused by the illuminant at wavelength λ_i. Since $I(\lambda_i)K'(\lambda_i)$ is a scalar, all $\Phi(\lambda, \lambda_i)$'s have the same shape as $J(\lambda)$. Considering the illuminant at all wavelengths, the overall observed spectrum is computed by summing up $\Phi(\lambda, \lambda_i)$'s for all wavelength λ_i, *i.e.*,

$$\Phi(\lambda) = \left(\int I(\lambda_i)K'(\lambda_i)\,\mathrm{d}\lambda_i \right) J(\lambda). \tag{2.3}$$

Note that the range of λ_i depends on the illuminant, and the range of λ is the range of the observed light we wish to measure. Equations 2.2 and 2.3 are not exact representations of the molecular physics of fluorescent objects, whose units are written in Watts instead of relative density. However, the results in Sun's [41] and Johnson's [23] work showed that the equations capture the properties of fluorescent objects well enough to improve the accuracy of object rendering.

2.2 Color Perception

Presenting an image to viewers with accurate color information is as important as producing an image with accurate colors. To properly present an image to viewers, we must understand how people perceive color.

Müller's zone theory is the current accepted theory of human color vision [33]. The process of perceiving color is divided into three zones. In the first zone, light is absorbed and converted into neural activity. The second zone is neural interaction on the retina, which consists of bipolar, horizontal and ganglion cells in addition to photoreceptors. This process generates neural signals, conveyed to the brain by the optical nerves. The third zone is located in the brain where the neural signals are interpreted, producing perception and action.

2.2.1 Chromatic Adaptation and Color Appearance Models

As mentioned in Section 2.1, the color of an object depends on the distribution of the spectrum it emits. Each emission spectrum covers a range of wavelengths, so the set of physical colors is thought of as an infinite dimensional space. Physiologically, each human cone cell is one of three types of photoreceptors, responding to light of relatively long (L), medium (M) and short (S) wavelengths (Figure 2.3). Therefore, we reduce the dimension of physical colors and model perceived colors using three cone responses: the extents to which each of the three types of cones is stimulated. Each cone response L, M or S, is a linear combination of three additive primaries called *tristimulus values*. Tristimulus values are the results of integrating emission spectrum with a set of *color matching functions* that specify the "unit amount" of tristimulus values at each wavelength. The computation of tristimulus values is outlined in Appendix B.

Cone responses are generated in the first zone in Müller's zone theory. Researchers discovered that these responses, or gain on the photoreceptors, are self-adjusted according to illumination conditions of the viewing environment. The process is called *chromatic adaptation*. Chromatic adaptation allows us to adapt to varying illumination conditions, thereby approximately preserve perceived color. The most widely accepted theory on chromatic adaptation was hypothesized by Johanne von Kries in 1890s, which states that during chromatic adaptation, the gain for each type of receptor scales independently. The physical change in the photoreceptors causes viewers' perception of color to change. To compensate for chromatic adaptation, researchers introduced *color appearance models (CAMs)*, which modify the displayed color of an image to provide the appearance adaptation would produce.

CAMs are based on a parameterized description of the viewing environment. For example, CIELAB [40], Hunt [21], Nayatani *et al.* [34], RLAB [11] and Fairchild's model [12] are earlier CAMs proposed by different researchers. von Kries hypothesis on chromatic adaptation is an important part of all these models. Fairchild studied the models in detail, comparing their performance under viewing conditions with different sources of illumination, luminous and background, *etc.* [6]. He concluded that, even though von Kries hypothesis is rudimentary and not usually known as a color appearance model itself, its predictions on changes in color

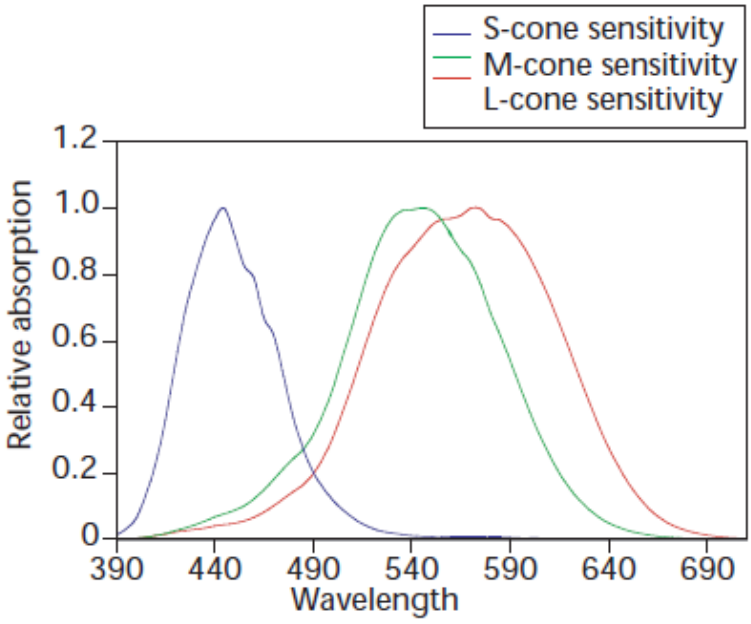

Figure 2.3: Response curves for human cone cell photoreceptors [23].

appearance are not much different than complex color appearance models. Luo *et al.* conducted a quantitative study on color appearance involving human subjects [30]. The result of the study was the LUTCHI data set containing 43,332 color appearance data points obtained under many viewing environments with different illuminants and luminance. Since then, most of the newly proposed CAMs, such as CIECAM02 [32], have been tuned to match the LUTCHI data set. CIECAM02 was created by a technical committee reporting to the International Commission on Illumination (CIE) in 2002. It is a unified model that supersedes the previous models. It is a complex model with many equations taking into account chromatic adaptation, surround luminance, brightness of illuminant, *etc.* , to predict the appearance of reproduced colors. Kim proposed a new CAM, also based on modified von Kries chromatic-adaptation model [26]. Even though Kim's model takes a different approach than CIECAM02 and their derivatives, its goal is still to match with LUTCHI data set as well as possible. The parameters in the model were obtained by curve-fitting, and the validity of the model when applying to displays were

shown using experiments. Lee's model [29] is another CAM based on curve-fitting the LUTCHI data set. Both Kim's and Lee's models are shown to match the LUTCHI color appearance data well.

2.2.2 Color Constancy

After chromatic adaptation, cone responses are conveyed to the brain by optical nerves. In the third zone in Müller's zone theory, the responses are interpreted. An important phenomenon that occurs during the interpretation is *color constancy*, in which the effect of illuminant portrayed within the displayed image is discounted from the perceived color. The term color constancy also refers to the mechanism for the discount of illuminant. The human color constancy mechanism consists of two components: estimating the illuminant and revising perceived color values based on the estimate. Color constancy is of great interest to researchers in realistic image reproduction for two reasons. First, color constancy algorithms can be used to remove unwanted color casts caused by illuminant; such process is called *white balance* in digital photography. Secondly, color constancy algorithms can be used to compute the *constant color descriptor* of an image under some reference illuminant. Such descriptor can be used to identify objects, or produce images of the same scene under other illuminants without re-rendering the scene. Existing color constancy algorithms are models of the human color constancy mechanism, and mainly differ in estimating the illuminant portrayed in the image. Some examples are

White-patch Retinex: Assume there is a white patch in the scene. The color of the illuminant is the color of the white patch [19].

Gray World: Assume that on average, the world is gray. The color of the illuminant is estimated as the average of the RGB channels for all pixels [20].

Gamut mapping: The set of all possible RGB (*i.e.*, gamut) due to surfaces in the scene under canonical illuminant is computed first. The color of the unknown illuminant is estimated as factors that map the gamut under this illuminant to the gamut under canonical illuminant [16,

15].

Statistics and machine learning: This group of methods uses techniques from machine learning and statistics such as Baysian network and neural network. They assume that the set of possible illuminants is known. To estimate the illuminant in a given image, every pixel is used to vote for the likelihood of each illuminant in the set [17, 18].

Many studies on comparing existing color constancy algorithms were done [10, 4, 5, 2], concluding that the algorithms all have significantly different approaches and performance. However, they share an important assumption: none of the objects in the image are fluorescent. In other words, the generic reflectance model in Equation 2.1 was used in all algorithms. Recently, researchers realized that such assumption limits the accuracy of color constancy algorithms. Barnard proposed ways to improve color constancy algorithms by including spectral data of several fluorescent objects [3]. His work was mainly based on experimental measurements and did not provide comprehensive models for fluorescent surfaces. Part of my research is to extend Barnard's work. By taking fluorescence into account, I am able to predict the color of objects under arbitrary illuminants more accurately than existing color constancy algorithms, and achieve better realism in color imaging.

2.3 Adaptive Displays

Once we have an image with accurate color information, we can consider implementing a color appearance model to display it accurately on self-luminous displays such as mobile phones, LCD monitors and TV's. Many color appearance models (CAMs) have been adopted by researchers in the display industry for building *adaptive displays*. An adaptive display has built-in sensors to detect changes in the viewing environment [1, 28]. For example, the LCD screen of an iMac G5^{TM} has a built-in ambient light sensor that detects changes in the brightness of the ambient. The screen is automatically dimmed when the ambient illumination decreases so that viewers do not experience a sudden contrast increase between screen brightness and surround brightness. However, this adaptive screen does not adjust the color of the displayed images to

account for chromatic adaptations, which makes it less perfect.

Many researchers studied how chromatic adaptation mechanism works when viewing adaptive displays with various surrounding conditions. In particular, Katoh *et al.* [25] and Seok *et al.* [39] pointed out that when looking at images on self-luminous displays, viewers are partially adapted to the displayed color image and partially to the ambient. As a result, a good CAM for adaptive displays must take into consideration both sources of adaptation.

It is also important to evaluate the performance of a CAM on actual displays. Park *et al.* [35] provided an evaluation of the original CIECAM02, as well as a refined version of CIECAM02 on a mobile display with seven human observers. He showed that the refined version had significant improvement in visual evaluation. Lee *et al.* [28] evaluated their own model on an HDTV with RGB sensors. They provided the schematics of integrated RGB sensors and concluded that the adjusted images had better visual quality. Lee *et al.*'s design of RGB sensors can be easily implemented in LCD displays, to work with other CAMs.

Chapter 3

Fluorescence in Color Images

Previous research in realistic color imaging discussed in Chapter 2 showed that traditional image reproduction algorithms have significant limitations, especially when dealing with fluorescent objects or surfaces. For instance, Figure 3.1(a) is an image seen under white light. The image consists of two fluorescent sheets (the flowers) on top of a non-fluorescent background image with ordinary reflective surfaces. If we want to predict what objects look like under green light without re-rendering the entire scene, we can relight the image using traditional relighting algorithms. For example, if we apply straightforward white-balance algorithm by adding green color cast to the entire image, we obtain an image in which the color of fluorescent objects, in particular, is not reproduced accurately (Figure 3.1(b) vs. Figure 3.1(c)). Other relighting or color constancy algorithms in previous research take similar approaches: various green cast would be added to the entire image without distinguishing between fluorescent and non-fluorescent objects.

The example above clearly shows that a pigmented surface's reflective and fluorescent components interact with illuminants differently. To achieve accurate relighting, it is necessary to separate the two components and process each component separately. This chapter presents a method for separating the reflective and fluorescent components of an image using unique properties of fluorescent surfaces.

(a) Test image under white light.

(b) Test image under green light predicted by traditional relighting algorithms.

(c) Test image under green light. (Ground truth).

Figure 3.1: Ground truth vs. relighted image produced by traditional relighting algorithm.

3.1 Properties of Fluorescent Surfaces

Section 2.1 showed that the emission spectrum of a fluorescent surface is, up to a constant, independent of its illuminant. Thus fluorescent surfaces have constant chromaticity when illumination condition varies. The proof of this property can be shown mathematically. We can compute the *tristimulus values* (see Appendix B) of a fluorescent surface from Equation 2.3 as

$$X = \int I(\lambda_i)K'(\lambda_i)\,\mathrm{d}\lambda_i \cdot \int \bar{x}(\lambda)J(\lambda)\,\mathrm{d}\lambda, \tag{3.1}$$

$$Y = \int I(\lambda_i)K'(\lambda_i)\,\mathrm{d}\lambda_i \cdot \int \bar{y}(\lambda)J(\lambda)\,\mathrm{d}\lambda, \tag{3.2}$$

$$Z = \int I(\lambda_i)K'(\lambda_i)\,\mathrm{d}\lambda_i \cdot \int \bar{z}(\lambda)J(\lambda)\,\mathrm{d}\lambda, \tag{3.3}$$

where $\bar{x}(\lambda), \bar{y}(\lambda), \bar{z}(\lambda)$ are the CIE color matching functions that specify the "unit amount" of tristimulus values at each wavelength, λ_i is integrated over the range of illuminant wavelength, λ is integrated over the range of visible light wavelength (380 nm to 720 nm), and $K'(\lambda_i)$ is defined in Equation 2.2. Let

$$X_0 = \int \bar{x}(\lambda)J(\lambda)\,\mathrm{d}\lambda,$$

$$Y_0 = \int \bar{y}(\lambda)J(\lambda)\,\mathrm{d}\lambda,$$

$$Z_0 = \int \bar{z}(\lambda)J(\lambda)\,\mathrm{d}\lambda,$$

be the *reference tristimulus values* of the normalized emission spectrum J. Substituting X_0, Y_0 and Z_0 into Equations 3.1 to 3.3, we have $X = kX_0$, $Y = kY_0$, and $Z = kZ_0$ with $k = \int I(\lambda_i)K'(\lambda_i)\,\mathrm{d}\lambda_i$. Note that k is a scalar and its value depends on the spectral power distribution of the illuminant and the excitation spectrum.

Now define *reference chromaticities* as

$$x_0 = \frac{X_0}{X_0 + Y_0 + Z_0},$$

$$y_0 = \frac{Y_0}{X_0 + Y_0 + Z_0}.$$

Figure 3.2: Fluorescent and non-fluorescent test surfaces. Left to right: red-orange, green-yellow, yellow-orange, cyan, yellow, red, green, purple.

Then the x-chromaticity of the object under an arbitrary illuminant becomes

$$\begin{aligned} x &= \frac{X}{X+Y+Z} \\ &= \frac{kX_0}{kX_0+kY_0+kZ_0} \\ &= \frac{X_0}{X_0+Y_0+Z_0} \\ &= x_0. \end{aligned}$$

Similarly, $y = y_0$. Thus the chromaticity of the fluorescent material is independent of both the illuminant and excitation spectrum; it only depends on the emission spectrum.

The claim of constant chromaticity was verified with experiments. The chromaticities of eight fluorescent and non-fluorescent surfaces (Figure 3.2) were measured under sixteen different illuminants using a spectrometer. The illuminants include four CIE standard daylights (Figure 3.3 Top), five indoor lights (Figure 3.3 Middle) and six random colored illuminants (Figure 3.3 Bottom). Table 3.1 shows the correlated color temperatures (CCT) of the CIE standard daylights and indoor lights.

Figure 3.4 shows the chromaticities-vs-illuminants plots of the experiments. The color of each line corresponds to the color of a test surface under white light. The plots show that as illuminants change, the chromaticities of fluorescent surfaces do not change as dramatically as reflective surfaces. Table 3.2 provides a more quantitative comparison. Under standard daylights, both x- and y-chromaticities of non-fluorescent surfaces on average vary twice as much as fluorescent surfaces. Table 3.3 shows that under random colored illuminants, the variation in x-chromaticities of non-fluorescent surfaces is twice as much as fluorescent surfaces, and the

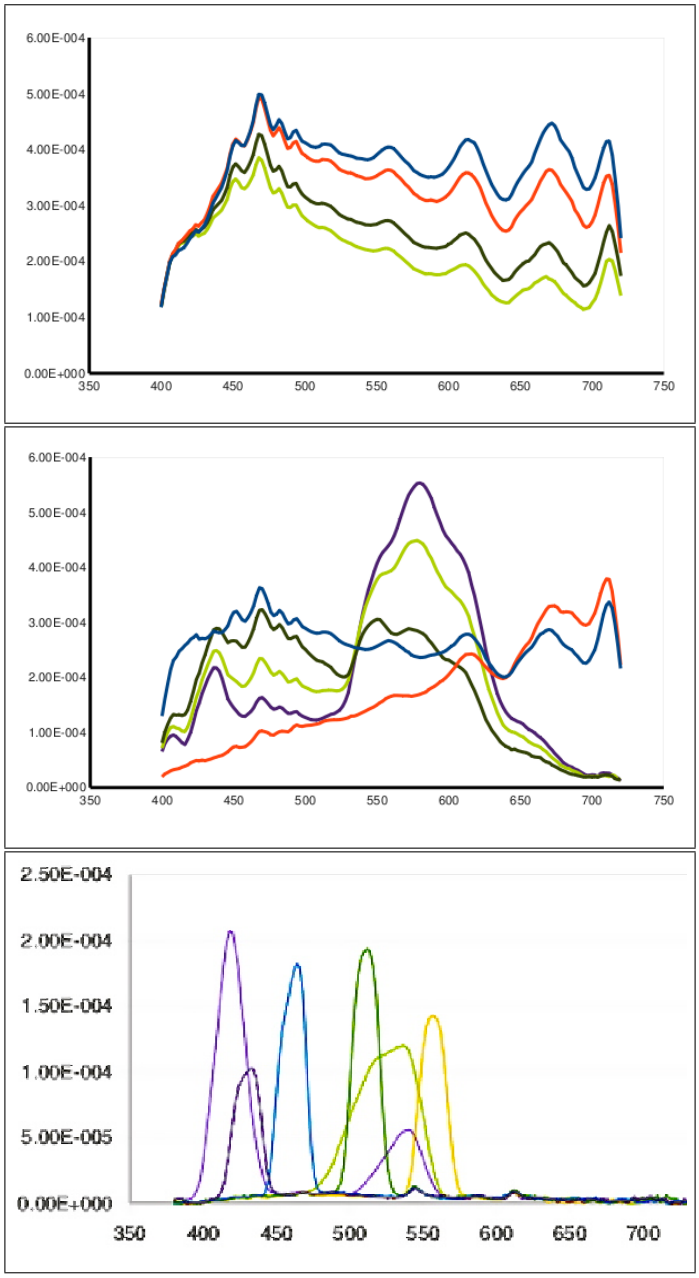

Figure 3.3: Illuminants used in verifying constant chromaticity. Top: four CIE standard daylights (D50, D55, D65, D75). Middle: five indoor lights (E, A, F1, F2, F3). Bottom: random colored lights.

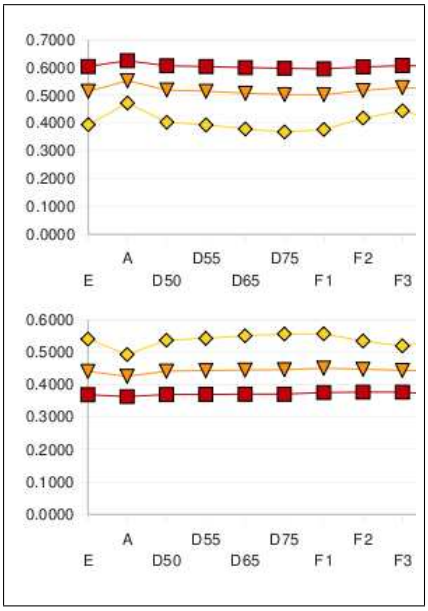

(a) Chromaticities of fluorescent surfaces vs. standard illuminants.

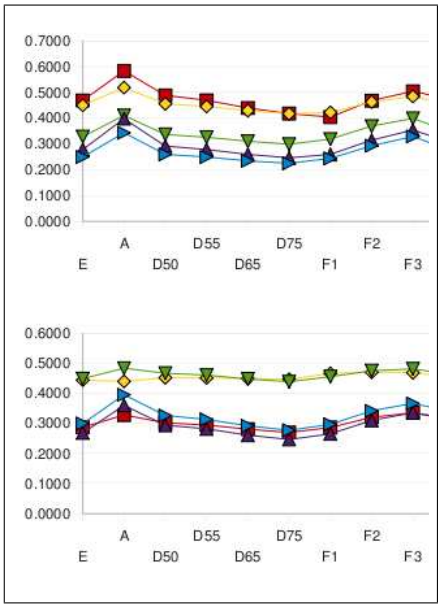

(b) Chromaticities of reflective surfaces vs. standard illuminants.

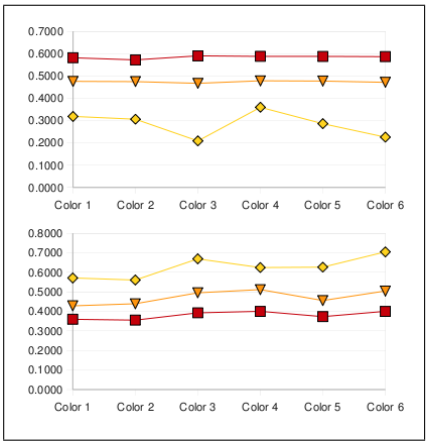

(c) Chromaticities of fluorescent surfaces vs. colored illuminants.

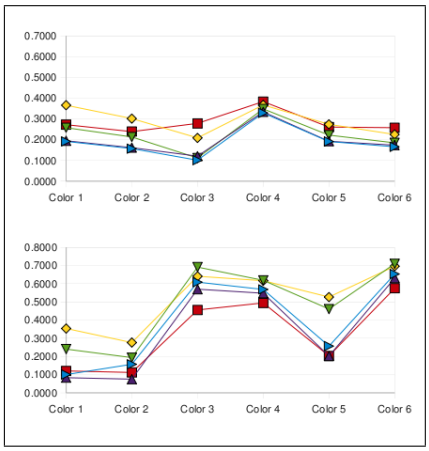

(d) Chromaticities of reflective surfaces vs. colored illuminants.

Figure 3.4: x-chromaticities (top) and y-chromaticities (bottom) plots for test surfaces under various illuminants.

Illuminant	Description	CCT(Kelvin)
E	Equal-energy white	5454
A	Incandescent/Tunsten	2856
D50	Horizon light	5003
D55	Mid-morning daylight	5503
D 65	Noon daylight	6504
D75	North sky daylight	7504
F1	Daylight fluorescent	6430
F2	Cool white fluorescent	4230
F3	White fluorescent	3450

Table 3.1: Descriptions and CCT's of CIE standard illuminants.

y-chromaticities varies more than five times. The fluorescent green-yellow surface has a greater variance than red-orange and yellow-orange surfaces because its excitation spectrum covers a narrower wavelength range; it exhibits strong fluorescence only for illuminants with much energy between 450 nm and 525 nm (Figure 2.2(b)). Some colored illuminants in the experiments have weaker intensity in the 450 nm to 520 nm range. Therefore, fluorescent green-yellow surface has a greater variance in color change than red-orange and yellow-orange surfaces.

The property of having constant chromaticity gives us a great way to distinguish fluorescence from reflectance. In the next section, a method for separating fluorescence from reflectance is presented.

Surfaces	**Maximum Difference (x,y)**	**Standard Deviation (x,y)**
Fluorescent		
Red-orange	(0.03, 0.01)	(0.008, 0.004)
Green-yellow	(0.11, 0.07)	(0.032, 0.018)
Yellow-orange	(0.05, 0.03)	(0.014, 0.006)
Average	**(0.06, 0.04)**	**(0.018, 0.010)**
Non-fluorescent		
Cyan	(0.12, 0.13)	(0.042, 0.025)
Yellow	(0.12, 0.03)	(0.032, 0.010)
Red	(0.21, 0.07)	(0.054, 0.023)
Green	(0.12, 0.07)	(0.038, 0.020)
Purple	(0.16, 0.12)	(0.046, 0.036)
Average	**(0.15, 0.08)**	**(0.042, 0.025)**

Table 3.2: Variations in the chromaticities under CIE standard daylights and indoor lights.

Surfaces	**Maximum Difference (x,y)**	**Standard Deviation (x,y)**
Fluorescent		
Red-orange	(0.02, 0.04)	(0.007, 0.020)
Green-yellow	(0.15, 0.14)	(0.057, 0.055)
Yellow-orange	(0.01, 0.08)	(0.004, 0.036)
Average	**(0.06, 0.09)**	**(0.023, 0.037)**
Non-fluorescent		
Cyan	(0.23, 0.55)	(0.076, 0.247)
Yellow	(0.16, 0.42)	(0.068, 0.169)
Red	(0.14, 0.46)	(0.052, 0.205)
Green	(0.24, 0.52)	(0.079, 0.226)
Purple	(0.21, 0.56)	(0.073, 0.259)
Average	**(0.12, 0.50)**	**(0.069, 0.221)**

Table 3.3: Variations in the chromaticities under random colored illuminants.

3.2 Separating Reflective and Fluorescent Components of an Image

Most relighting algorithms work on RGB-specified images rather than spectrally-specified ones. Therefore it is important to have a method for identifying the fluorescent component of an image taken by regular cameras. A regular charged-couple device (CCD) camera has three color channels: Red (R), Green (G) and Blue (B). The color of each pixel on the image taken by a CCD camera, p, is computed as the sum of the colors for all three channels, *i.e.*,

$$p = p_R + p_G + p_B.$$

Let p_c be the color of a pixel for channel c where $c = \{R, G, B\}$. Then for an image of objects with both reflective and fluorescent components, p_c is computed as the sum of the color for reflective component $p_{c,O}$ and the fluorescent component $p_{c,F}$, *i.e.*,

$$p_c = a_c p_{c,O} + b_c p_{c,F}. \tag{3.4}$$

As the illumination changes, the contribution to the appearance of the object from the reflective and fluorescent components changes. Let a_c and b_c be the coefficients to represent the amount of contribution from each component to the pixel color p_c. a_c and b_c depend on the interactions between each component and the illuminant. Now the color of a pixel for each channel, p_c, is represented as a linear combination of the reflective component $p_{c,O}$ and fluorescent component $p_{c,F}$. Both are unknown. The spectral distribution of the illuminant under which p is taken, is also unknown. To tackle the problem of blindly separating the two components when only the set of pixel colors, $\{p\}$ are known, I assume that the two components are independent. This assumption is reasonable since in the absence of image interpretation, the spatial distribution of the fluorescent component is uncorrelated to the spacial distribution of the reflective component. Farid and Adelson proposed an effective algorithm for blind component separation of an image: they used independent component analysis (ICA) [22] to separate a painting from a reflection on the glass covering the painting [14]. The fluorescent component of an image is analogous to the painting itself in Farid and Adelson's problem, and the reflective component is analogous to the reflection of an observer off the glass. By applying ICA [1], I successfully

[1]The FastICA package in MATLAB is used in the experiments.

separated the reflective and fluorescent component of an image using images of the scene taken under two different illuminants. The algorithm is applied independently to each of the three RGB channels of the input images. The separation results are six images: three for each component. The examples are shown in Chapter 5.

3.3 New Approach in Relighting Images

The ability to separate the ordinary reflective and fluorescent components of an image provides an improved method for relighting images. Traditional relight algorithms relight an image uniformly, *i.e.,*

$$\text{original image} \xrightarrow{\text{relighting}} \text{new image.}$$

The new approach, on the other hand, relights only the reflective component and preserves the fluorescent component, *i.e.,*

$$\text{original image} \left\{ \begin{array}{l} \text{reflective component} \\ \text{fluorescent component} \end{array} \right. \xrightarrow{\text{relighting}} \text{new reflective component} \Bigg\} \text{new image}$$

Figure 3.5 shows the result produced by the new approach. Compared to the result produced by traditional relighting algorithms (Figure 3.1) at the beginning of the chapter, it is evident that the new approach produces an output image with more accurate color.

(a) Test image under white light.

(b) Test image under green light predicted by the new approach.

(c) Test image under green light. (Ground truth).

Figure 3.5: Ground truth vs. relighted image produced by the new approach.

Chapter 4

Adaptation and a New Model for Adaptive Displays

The previous chapter discussed how to improve the presentation of images that are partly fluorescent. In this chapter, I will show my research in how to present the images on self-luminous displays accurately. As mentioned in Chapter 2, many color appearance models have been proposed for preserving the color appearance of displayed images. However, these models are both complicated and focusing on fitting experimental data. In this chapter, I propose a model which takes into account viewers' adaptation of the displayed content itself in addition to the ambient illumination. The model is developed in three stages. First, we consider how viewers look at and adapt to the displayed image. Then, we take chromatic adaptation into account. Last, we apply the inverse of von Kries model, adjusting the displayed image to maintain its color appearance.

Many matrices, square and rectangular, are used in deriving the model. To simplify the notation, this chapter uses the Einstein notation (Appendix A).

4.1 Internal Illumination

Suppose the reflectance at point x on the image is $R^\lambda(x)$, where $R^\lambda(x)$ is a continuous function on the wavelength domain, and suppose the scene illuminant, I^μ is similar. λ and μ are usually sampled in the visible light range, 380 nm to 720 nm, since human eyes respond to lights in this range. For convenience, write the reflectance as a diagonal matrix, $R^\lambda_\mu(x)$. Then the light emitted from the image at point x is $R^\lambda_\mu(x)I^\mu$. Then the tristimulus values at point x, $\mathbf{X}^i(x)$, are

$$\mathbf{X}^i(x) = \bar{x}^i_\lambda R^\lambda_\mu(x) I^\mu,$$

where $\bar{x}^i_\lambda$ are the color matching functions for $i = \{X, Y, Z\}$.

At point x on the display, the light emitted is $S^\lambda(x)$, which is the sum of the normalized primaries, P^λ_a, where $a = \{R, G, B\}$, times the *excitations*[1], $e^a(x)$:

$$S^\lambda(x) = P^\lambda_a e^a(x).$$

The corresponding tristimulus values are

$$\mathbf{Y}^i(x) = \bar{x}^i_\lambda P^\lambda_a e^a(x) = p^i_a e^a(x),$$

where we define p^i_a as the *primary chromaticities*, the property of a self-luminous display which can be found when calibrating the display [9].

Assume that there is no excess chromatic adaptation. In other words, the viewer's chromatic adaptation is determined by the illuminant in the scene (Figure 4.1). We want to choose excitations $e^a(x)$ so that the light entering the viewer's eyes has the same tristimulus values as the colors of the image. In other words,

$$\mathbf{X}^i(x) = \mathbf{Y}^i(x),$$

which entails

$$\mathbf{X}^i(x) = \bar{x}^i_\lambda R^\lambda_\mu(x) I^\mu = p^i_a e^a(x). \tag{4.1}$$

[1] *e.g.* ,the "amount" of primaries

$\mathbf{X}^i(x)$ are known from the image and p_a^i from display calibration. The unknown excitations, $e^a(x)$, are

$$e^a(x) = (p^{-1})_i^a \bar{x}_\lambda^i R_\mu^\lambda(x) I^\mu, \tag{4.2}$$

where $p_a^i (p^{-1})_j^a = \delta_j^i$ defines the inverse matrix of primary chromaticities. δ_j^i is the Kronecker delta[2].

4.2 Chromatic Adaptation

In the previous section, we assumed that the viewer is adapted to the illumination in the scene from which the image was generated. We apply the zone theory in Section 2.2 to compute the color in the presence of adaptation. The zone theory of color vision asserts that there is a *cone response matrix*, M_r^i, where $r = \{L, M, S\}$ and $i = \{X, Y, Z\}$, that maps the tristimulus values (XYZ) to cone signals (LMS) in the photoreceptors. The entries in the matrix M_r^i were determined experimentally decades ago by various researchers. A standardized matrix is used in the CIECAM02 color appearance model [32]. Since tristimulus values are linear functions of color matching functions, we can assume that the same cone response matrix is used to transform color matching functions into spectral sensitivities of cones with respect to light at the surface of the cornea. Define *spectral sensitivities of cones* to be

$$\bar{c}_\lambda^r = M_i^r \bar{x}_\lambda^i.$$

In the case where the illumination of the viewing environment is different from the scene illuminant, the state of adaptation of the viewer is jointly determined by the two illuminants. We use the von Kries model [13] to capture the effect of adaptation. According to the von Kries model, the effect of chromatic adaptation is to scale the gain at the each type of cone cell receptor. Thus we have

$$\bar{c}_\lambda^r = \alpha_s^r \bar{c}_\lambda^s, \tag{4.3}$$

[2] $\delta_j^i = 1$ if $i = j$, $\delta_j^i = 0$ otherwise.

where α_s^r is the diagonal von Kries adaptation matrix. In most color appearance models, the diagonal entries of α are computed as L_{max2}/L_{max1}, M_{max2}/M_{max1} and S_{max2}/S_{max1}, where the numerators are the cone responses for white point[3] of the illuminant in the adapted viewing environment, and the denominators are the cone responses for the white point of the original viewing condition [12].

The original color matching functions $\bar{x}_\lambda^i$ then change to new *adapted color matching functions*, $\underset{\sim}{\bar{x}}_\lambda^i$, where

$$\underset{\sim}{\bar{x}}_\lambda^i = (M^{-1})_r^i \alpha_s^r M_j^s \bar{x}_\lambda^j,$$

with the inverse matrix defined by $(M^{-1})_s^i M_j^s = \delta_j^i$.

Using the adapted color matching functions, the adapted tristimulus values, $\mathbf{Z}^i(x)$, of the light emitted from the display at point x are

$$\begin{aligned} \mathbf{Z}^i(x) &= (M^{-1})_r^i \alpha_s^r M_j^s \bar{x}_\lambda^j P_a^\lambda e^a(x) \\ &= (M^{-1})_r^i \alpha_s^r M_j^s p_a^j e^a(x) \\ &= \underset{\sim}{p}_a^i e^a(x), \end{aligned}$$

where the *adapted primary chromaticities* are

$$\underset{\sim}{p}_a^i = (M^{-1})_r^i \alpha_s^r M_j^s p_a^j. \tag{4.4}$$

Thus, $\underset{\sim}{p}_a^i$ can be computed from the primary chromaticities. The excitations $e^a(x)$ can be computed with Equation 4.2 in the previous section.

In Section 4.1, the tristimulus values of point x on the image were computed to be $\mathbf{X}^i(x) = p_a^i e^a(x)$. But the viewer perceives the adapted tristimulus values $\mathbf{Z}^i(x)$, a different color than the tristimulus values on the image $\mathbf{X}^i(x)$ (Figure 4.2). Therefore achieving constancy in color appearance requires the new excitation $\underset{\sim}{e}^a(x)$ such that

$$\underset{\sim}{p}_a^i \underset{\sim}{e}^a(x) = p_a^i e^a(x). \tag{4.5}$$

The new tristimulus values of the light emitted from the display are $p_a^i \underset{\sim}{e}^a(x)$, which are called the *adjusted tristimulus values* (Figure 4.3).

[3]The tristimulus values of a “white" surface under the illuminant.

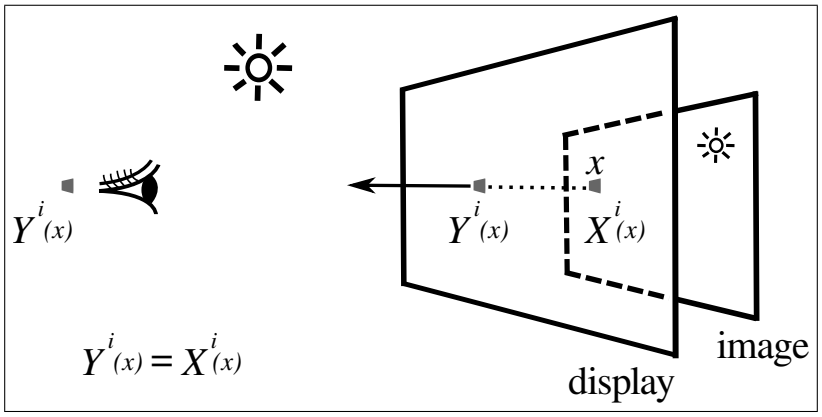

Figure 4.1: The illuminant in the viewing environment is the same as the scene illuminant. No adaptation occurs. The color perceived by our brain is the same as the displayed color ($\mathbf{Y}^i$), so we can observe the true color ($\mathbf{X}^i$).

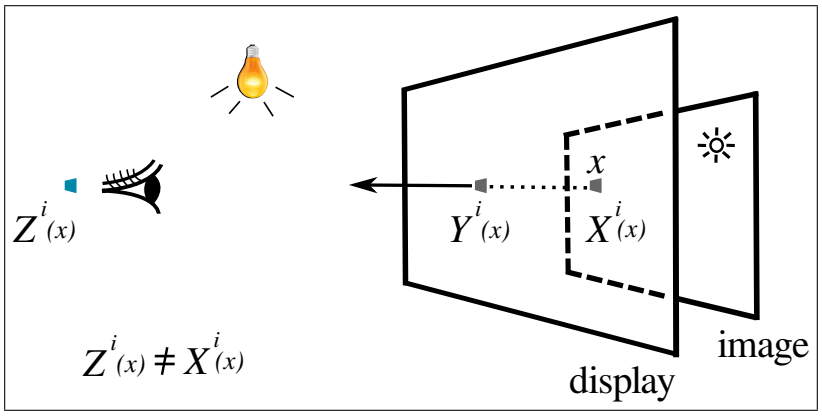

Figure 4.2: When the illuminant in the viewing environment is not the same as the scene illuminant, chromatic adaption causes the color perceived by our brain ($\mathbf{Z}^i$) to be different from the displayed color ($\mathbf{Y}^i$), so we cannot observe the true color ($\mathbf{X}^i$).

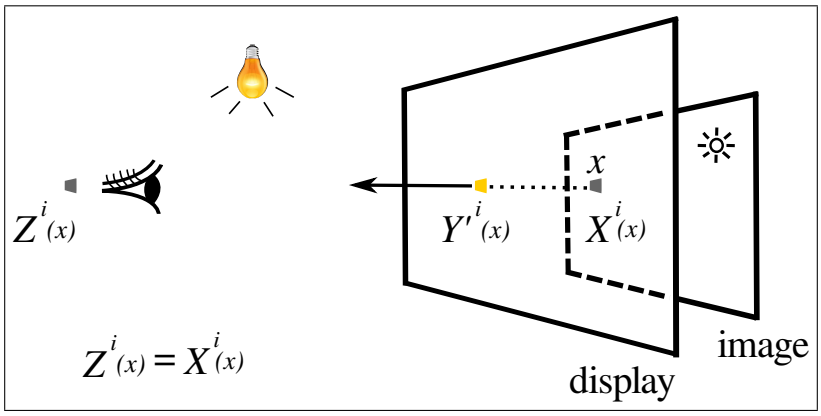

Figure 4.3: To compensate for adaptation, we must adjust the displayed color (to $\mathbf{Y}'^i$) so that the color received by our brain ($\mathbf{Z}^i$) is the same as the true color ($\mathbf{X}^i$).

4.3 von Kries Model

The goal is to solve for the new excitations $\underset{\sim}{e}^a(x)$ such that Equation 4.5 holds. By substituting the adapted primary chromaticities in Equation 4.4, we obtain

$$(M^{-1})^i_r \alpha^r_s M^s_j p^j_a \underset{\sim}{e}^a(x) = p^i_a e^a(x).$$

Thus

$$\underset{\sim}{e}^a(x) = (p^{-1})^a_j (M^{-1})^j_s (\alpha^{-1})^s_r M^r_i p^i_a e^a(x). \tag{4.6}$$

Substituting Equation 4.1, we have

$$\underset{\sim}{e}^a(x) = (p^{-1})^a_j (M^{-1})^j_s (\alpha^{-1})^s_r M^r_i X^i(x),$$

and the adjusted tristimulus values are

$$\begin{aligned} p^i_a \underset{\sim}{e}^a(x) &= p^i_a (p^{-1})^a_j (M^{-1})^j_s (\alpha^{-1})^s_r M^r_i X^i(x) && (4.7) \\ &= (M^{-1})^j_s (\alpha^{-1})^s_r M^r_i X^i(x). && (4.8) \end{aligned}$$

Equation 4.8 shows that the adjusted tristimulus values at point x can be easily computed by applying an inverse von Kries adaptation matrix to our cone responses to the original image.

The proof in the next section shows that this model is valid when used to adjust the displayed image to provide a uniform viewing experience.

4.4 Validity of von Kries Model

As mentioned in Section 4.2, the viewer's state of adaptation is controlled jointly by the illumination of the viewing environment and the scene illuminant. Therefore to show the validity of von Kries model, we reformulate the problem to take into account the scene illuminant as well.

4.4.1 Reformulation of the Problem

In Section 4.3, we substituted one equality $\mathbf{X}^i(x) = p_a^i e^a(x)$ in Equation 4.1 into Equation 4.6 to derive the von Kries model which only involves primary chomaticities and excitations. If we substitute the other equality $\mathbf{X}^i(x) = \bar{x}_\lambda^i R_\mu^\lambda(x) I^\mu$ in Equation 4.1 to Equation 4.5, we obtain

$$\underset{\sim}{p}_a^i \underset{\sim}{e}^a(x) = \bar{x}_\lambda^i R_\mu^\lambda(x) I^\mu. \tag{4.9}$$

Paralleling Equation 4.2, $\underset{\sim}{e}^a(x)$ is

$$\underset{\sim}{e}^a(x) = (p^{-1})_i^a \bar{x}_\lambda^i R_\mu^\lambda(x) \underset{\sim}{I}^\mu,$$

where $\underset{\sim}{I}^\mu$ is a new scene illuminant, chosen so that the tristimulus values on the display undo the effect of the viewer's adaptation to the illuminant in the viewing environment.

Substitute $\underset{\sim}{p}_a^i$ in Equation 4.4 and $\underset{\sim}{e}^a(x)$ to Equation 4.9

$$\begin{aligned}
(M^{-1})_r^i \alpha_s^r M_j^s \underset{\sim}{p}_a^j \underset{\sim}{e}^a(x) &= \bar{x}_\lambda^i R_\mu^\lambda(x) I^\mu && (4.10)\\
(M^{-1})_r^i \alpha_s^r M_j^s \underset{\sim}{p}_a^j (p^{-1})_i^a \bar{x}_\lambda^i R_\mu^\lambda(x) \underset{\sim}{I}^\mu &= \bar{x}_\lambda^i R_\mu^\lambda(x) I^\mu && (4.11)\\
(M^{-1})_r^i \alpha_s^r M_j^s \bar{x}_\lambda^j R_\mu^\lambda(x) \underset{\sim}{I}^\mu &= \bar{x}_\lambda^i R_\mu^\lambda(x) I^\mu && (4.12)\\
\alpha_s^r M_j^s \bar{x}_\lambda^j R_\mu^\lambda(x) \underset{\sim}{I}^\mu &= M_i^r \bar{x}_\lambda^i R_\mu^\lambda(x) I^\mu && (4.13)
\end{aligned}$$

In the equation above, the known values are the coefficients in the von Kries adaptation matrix α_s^r, the cone response matrix M_j^s (and M_i^r), and the color matching functions $\bar{x}_\lambda^j$ (and $\bar{x}_\lambda^i$). The reflectance, $R_\mu^\lambda(x)$, is unknown since we cannot always predict what object is shown in the image. I^μ is the original scene illuminant. We have no way to predict it; however later on, we are able to show that by making reasonable assumptions, it is irrelevant. $\underset{\sim}{I}^\mu$ and $R_\mu^\lambda(x)$ are the unknowns. We assume the image is uniformly illuminated and it is impossible to obtain the reflectance R_μ^λ for every single point x on the image. Thus the goal is to find a new scene illuminant, $\underset{\sim}{I}^\mu$, that is independent of the reflectance $R_\mu^\lambda(x)$ so that Equation 4.13 holds.

4.4.2 Solve for a New Scene Illuminant

To solve for a new scene illuminant $\underset{\sim}{I}^\mu$, we first write I^μ and $\underset{\sim}{I}^\mu$ as a linear combination of basis functions for illuminants. Judd *et al.* [24] and Romero *et al.* [37] showed that there exist basis functions for illuminants that cover most outdoor (daylight) and indoor lights, such that any illuminant can be written as a linear combination of the basis functions. Thus we have

$$I^\mu = m^k I_k^\mu,\ \underset{\sim}{I}^\mu = \underset{\sim}{m}^k I_k^\mu, \tag{4.14}$$

where I_k^μ is the k^{th} basis function for illuminants. m^k and $\underset{\sim}{m}^k$ are the k^{th} coefficients for $k = \{1,2,3\}$.

Cohen [8] showed that there exist basis functions for the Munsell color chips with 1296 colors. The Munsell color chips are considered to span the set of reproducible colors in most images [38]. Therefore we can write the reflectance at point x of an image as a linear combination of the basis functions for the Munsell color chips, *i.e.*,

$$R_\mu^\lambda(x) = n^l(x)(R_l)_\mu^\lambda,$$

where $(R_l)_\mu^\lambda$ is the l^{th} basis function for the Munsell color chips, and $n^l(x)$ is the l^{th} coefficient for $l = \{1,2,3\}$. Now Equation 4.13 can be written as

$$\alpha_s^r M_j^s \bar{x}_\lambda^j \left(n^l(x) R_{l,\mu}^\lambda\right)\left(\underset{\sim}{m}^k I_k^\mu\right) = M_i^r \bar{x}_\lambda^i \left(n^l(x) R_{l,\mu}^\lambda\right)\left(m^k I_k^\mu\right).$$

Let $Q^{\lambda}_{l,k} = R^{\lambda}_{l,\mu}(x) I^{\mu}_{k}$ be the spectral power distribution of the l^{th} reflectance basis interacting with the k^{th} illuminant basis. Then we have

$$\begin{aligned} \alpha^{r}_{s} M^{s}_{j} \bar{x}^{j}_{\lambda} n^{l}(x) Q^{\lambda}_{l,k} \underset{\sim}{m}^{k} &= M^{r}_{i} \bar{x}^{i}_{\lambda} n^{l}(x) Q^{\lambda}_{l,k} m^{k}, \\ \alpha^{r}_{s} \Psi^{s}_{k} \underset{\sim}{m}^{k} &= \Psi^{r}_{k} m^{k}, \end{aligned}$$

if $\Psi^{s}_{k} = M^{s}_{j} \bar{x}^{j}_{\lambda} n^{l}(x) Q^{\lambda}_{l,k}$ and $\Psi^{r}_{k} = M^{r}_{i} \bar{x}^{i}_{\lambda} n^{l}(x) Q^{\lambda}_{l,k}$. Therefore

$$\underset{\sim}{m}^{k} = (\Psi^{-1})^{k}_{b} (\alpha^{-1})^{b}_{r} \Psi^{r}_{k} m^{k}, \tag{4.15}$$

where $\Psi^{s}_{k} (\Psi^{-1})^{k}_{b} = \delta^{s}_{b}$ and $\alpha^{r}_{s} (\alpha^{-1})^{b}_{r} = \delta^{b}_{s}$. By finding $\underset{\sim}{m}^{k}$, we can use Equation 4.14 to find $\underset{\sim}{I}^{\mu}$. Figure 4.4(a) shows that when the viewing condition changes from equal-energy illuminant (E) to incandescent light (A), the values of the new illuminant computed from 1296 different colors from the Munsell color chips converge to the same number. The routine can be easily implemented in MATLAB® (Appendix E). The solution to solving for new scene illuminant, written in full matrix form, can be found in Appendix C.

The result shows that we can find a single, uniform illuminant to re-illuminate the scene so that the color appearance of the image is preserved. Figure 4.4(b) shows a similar plot for new scene illuminant when the viewing condition changes from E to cyan light (RGB= $[94, 243, 255]$). In other words, applying an inverse von Kries model has the same effect as theoretically re-illuminating the image to compensate for viewer's adaptation. The proposed model was shown to be suitable for adaptive displays.

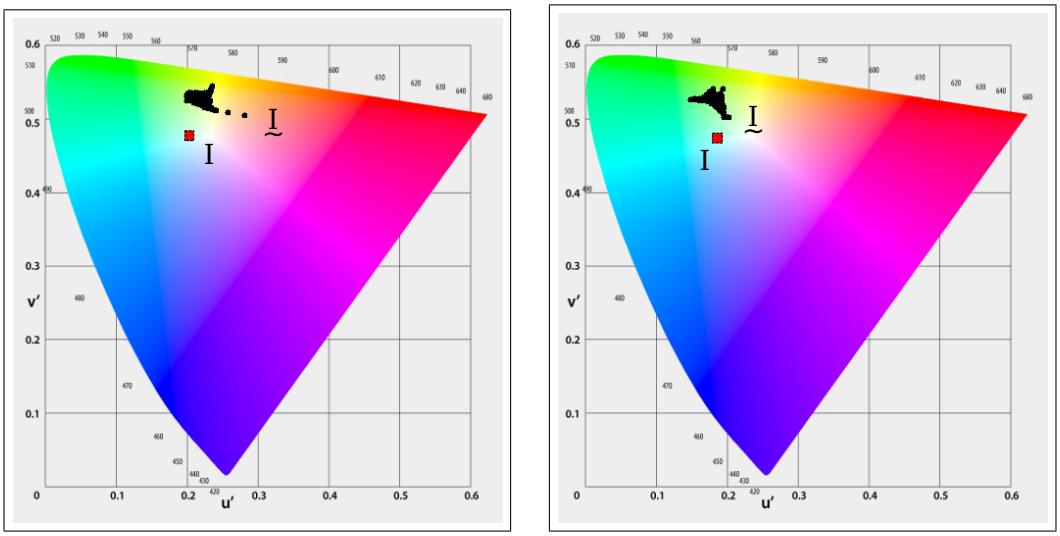

(a) Illuminant changes from illuminant E to A

(b) Illuminant changes from illuminant E to cyan light

Figure 4.4: Values of the new scene illuminant computed from 1296 Munsell color chips (black dots), for different changes in viewing conditions. The values converge to a single value.

Chapter 5

Results and Discussion

5.1 Image Separation and Relighting

Independent component analysis (ICA) is used to separate and relight several test images of fluorescent objects taken by an ordinary CCD camera. The first image consists of colored sheets. The sheets contain different amount of fluorescence and reflectance (Figure 5.1 Top). The two flowers at the top are fluorescent, appearing green-yellow and red-orange under white illumination. The flower in the middle and the leaves at the bottom are non-fluorescent, with dark red and dark green reflectances.

The fluorescent and reflective components were recovered from images taken under a blue illuminant and a yellow illuminant (Figure 5.2(a)). The recovered fluorescent component (Figure 5.2(b)) shows that the color of fluorescent component of the green-yellow fluorescent sheet is in fact green. The measured emission spectrum of the sheet (Figure 2.2(b)) suggests that the color of the fluorescent component is indeed green. Furthermore, images of the fluorescent flowers were taken under UV light, which provided ground truth for the color of the fluorescent component (Figure 5.1 Bottom). The recovered appearance agrees with experimental results, as well as the ground truth. The dark red and dark green sheets used in making the scene have ordinary reflectance only since the color of the middle flower and the leaves in the

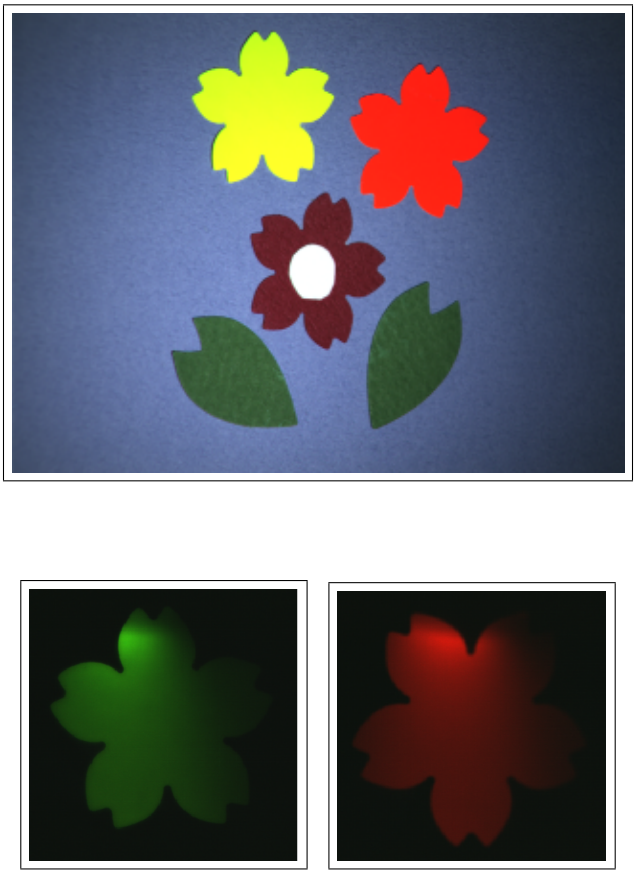

Figure 5.1: Top: colored sheets under white light. Bottom: fluorescent sheets under UV light.

recovered reflective component (Figure 5.2(c)) is the same as the color under white illuminant (flower and leaves at the bottom of Figure 5.1). It is also worth noting that the green-yellow fluorescent flower appears to be reddish orange in the recovered image of the reflective component. Combining the reddish orange color with the green color in the fluorescent component gives the flower its yellow appearance.

ICA is effective on scenes with complex color patterns, and scenes that consist of real objects. Figure 5.3 consists of two fluorescent flowers placed over a non-fluorescent background image with complex color patterns. The proposed method succeeds in identifying the green and red-orange color of the fluorescent sheets. The recovered image of the fluorescent component

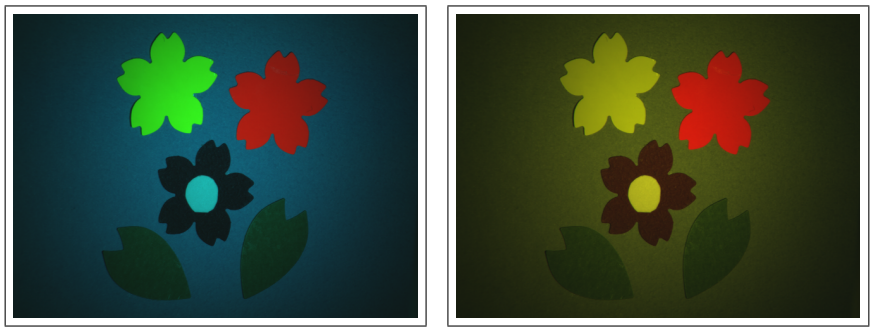

(a) Input test images (under blue and yellow illuminants).

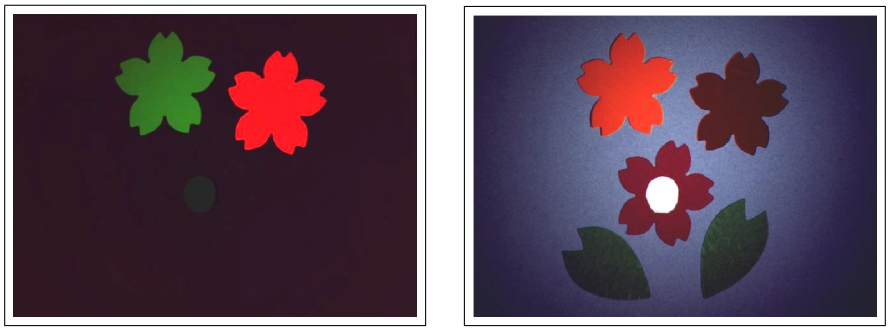

(b) Image of the fluorescent component. (c) Image of the reflective component.

Figure 5.2: Recovered fluorescent and reflective components using images taken under blue and yellow illuminants.

(a) Test Image under white light.

(b) Input test images (under green and pink illuminants).

(c) Image of the fluorescent component.

(d) Image of the reflective component.

Figure 5.3: Fluorescent and reflective components of an image with complex color patterns.

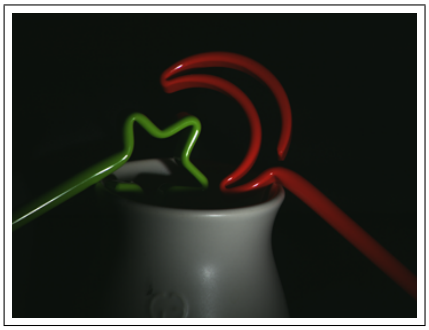

(a) Test image under white light.

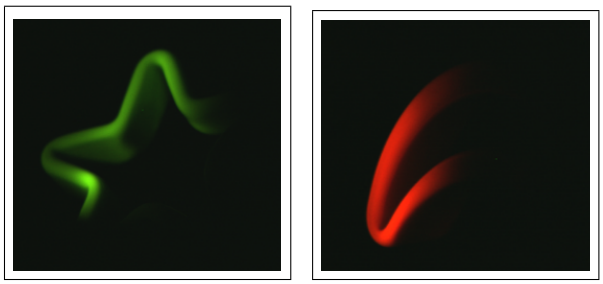

(b) Fluorescent sticks (with different orientation) under UV light.

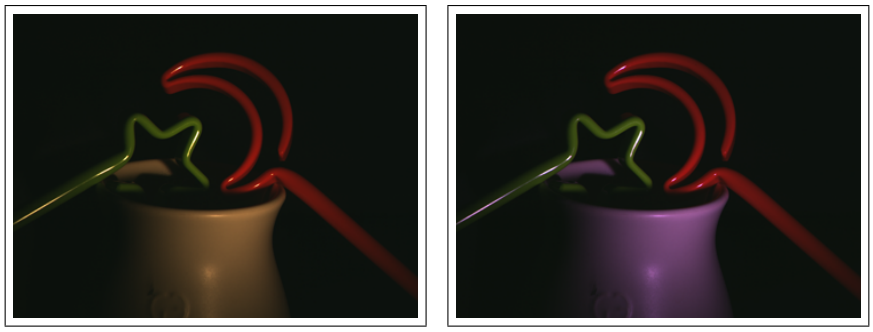

(c) Input test images (under yellow and purple illuminants).

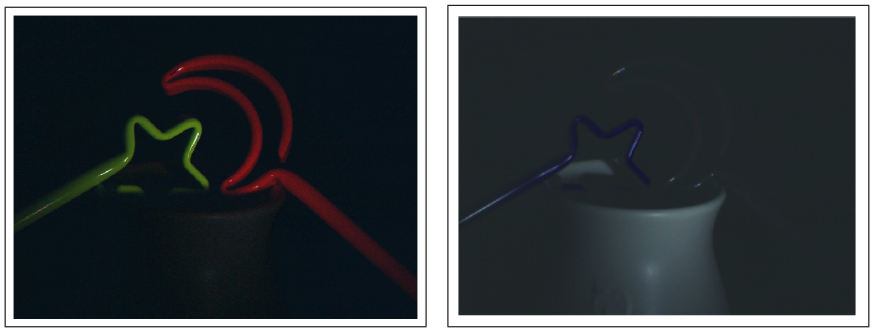

(d) Recovered images of the fluorescent and reflective components.

Figure 5.4: Fluorescent and reflective components of an image with real objects.

(Figure 5.3(c)) excludes the background image completely, which demonstrates the correctness and effectiveness of the separation. Figure 5.4 shows the recovered results for a scene consisting of real objects. The fluorescent sticks and non-fluorescent jar are separated into two images. The color of the sticks (Figure 5.4(d)) matches with the ground truth (Figure 5.4(b)).

5.2 Comparison of New Model for Adaptive Displays with Existing Models

An application was written to simulate an adaptive display, so as to compare the proposed model for adaptive displays with other color appearance models (Figure 5.5(a)). The standard illuminant is equal-energy white illuminant (E). The color of the new illuminant is changed using sliders (Figure 5.5(b)). Four models, CIECAM02, Fairchild's model, CIELAB, and our model (von Kries) are compared under two sets of illuminant changes. First, the illuminant changes from equal-energy (E) to incandescent (A), which has orange-yellow color. Then the illuminant changes from E to cyan. The algorithms for the four models are provided in Appendix D.

Nine colors were selected to compare the adjusted colors under the new illumination. Figure 5.6 shows the results for four colors: red, green, blue and yellow. Figure 5.7, 5.8 and 5.9 show the adjusted colors on the $u'v'$ diagram. Visually the adjusted colors from CIECAM02, Fairchild's model and von Kries model are similar. The $u'v'$ plots (Figure 5.10) show the closeness in chromaticities of the adjusted colors. The adjusted images produced by CIELAB appear different than the others, which agrees with the conclusions of other studies [6].

In my study, I focused on comparing the predictions of the proposed model with existing models. The comparison of von Kries model with psychophysical data was previously done by Fairchild [13]. Fairchild compared the predictions of von Kries model with the experimental data obtained by Breneman [7]. The vector fields (*i.e.,* direction of arrows) of Fairchild's results (Figure 5.11) agree with the results of my simulation (Figure 5.7, 5.8 and 5.9), implying that von Kries model produces comparable results both in theory and in practice.

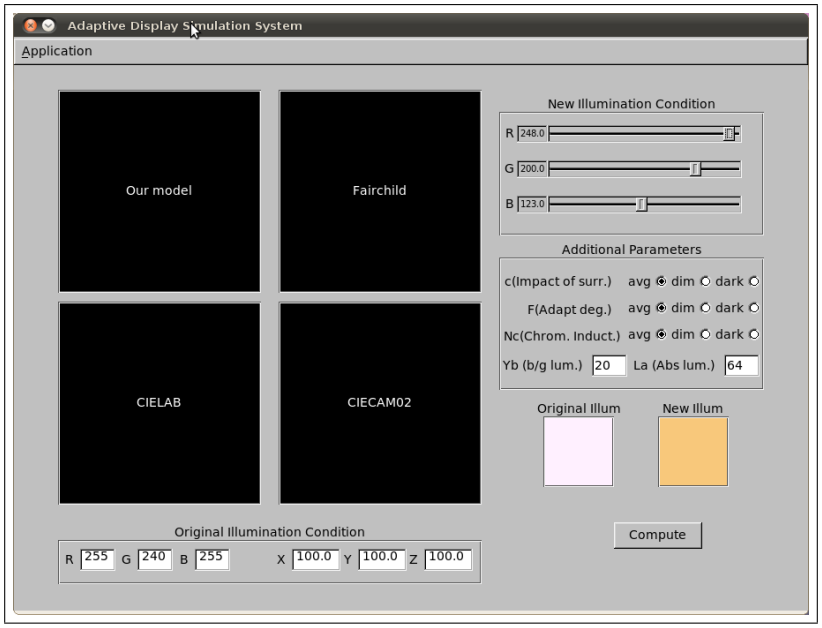

(a) User interface of the adaptive display simulation system.

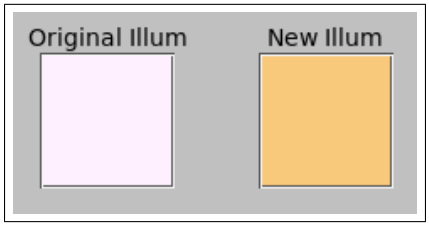

(b) Panels showing color of illuminants. The color of the original illuminant and the new illuminant can be modified using sliders.

Figure 5.5: Adaptive display simulation system.

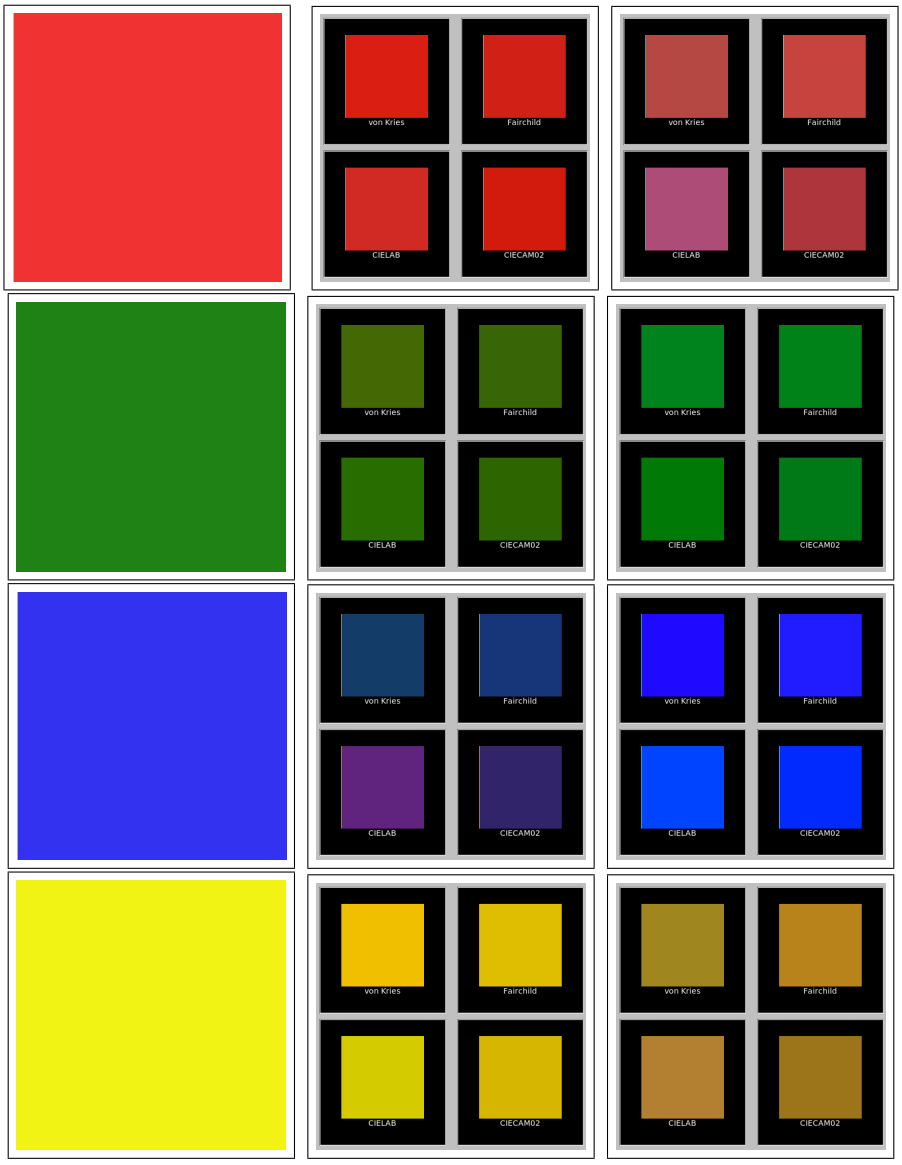

Figure 5.6: Color changes predicted by four models (Top to bottom: von Kries, Fairchild's, CIELAB, CIECAM02). Left column: colors under E. Middle column: adjusted colors for displaying under A. Right column: adjusted colors for displaying under cyan illuminant.

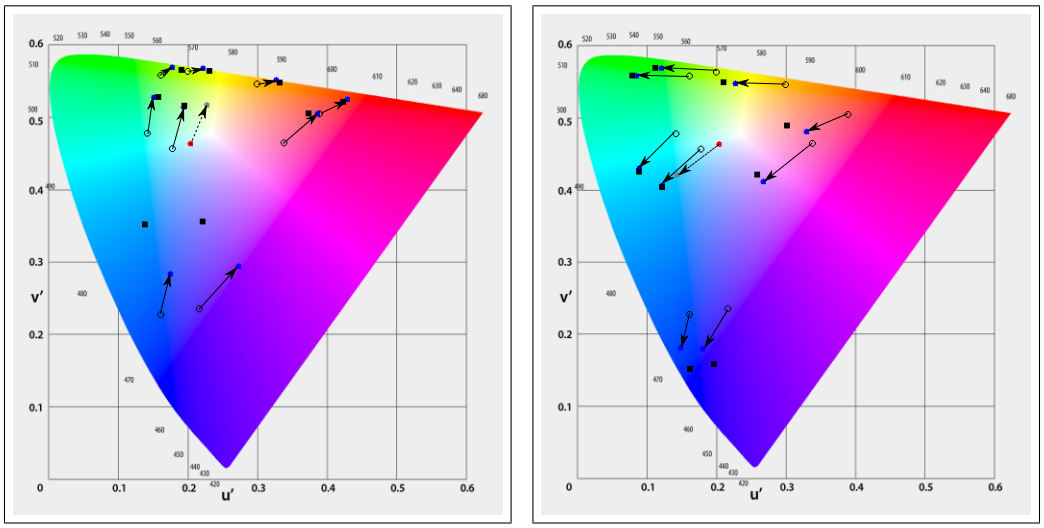

Figure 5.7: Color changes predicted by CIECAM02 and von Kries model on the CIE $u'v'$ diagram. Red dots: original illuminant. Gray dots: new illuminant. Black dots: predictions of CIECAM02. Blue dots: predictions of von Kries model.

The results computed by four models were also compared for input images with more complex color patterns. Figure 5.12 shows the original images under illuminant E. Figure 5.13 to Figure 5.16 are the adjusted images under illuminant A and the cyan illuminant. It is evident that when input images are more colorful and complex, it is no longer possible to see significant difference between images predicted by different models.

Figures 5.7, 5.8 and 5.9 show that when the illuminant changes, the changes in tristimulus values are large, many times larger than visual thresholds. Thus, when accurate color appearance is important, such as while reading this paper, taking these adaptation effects into account is important.

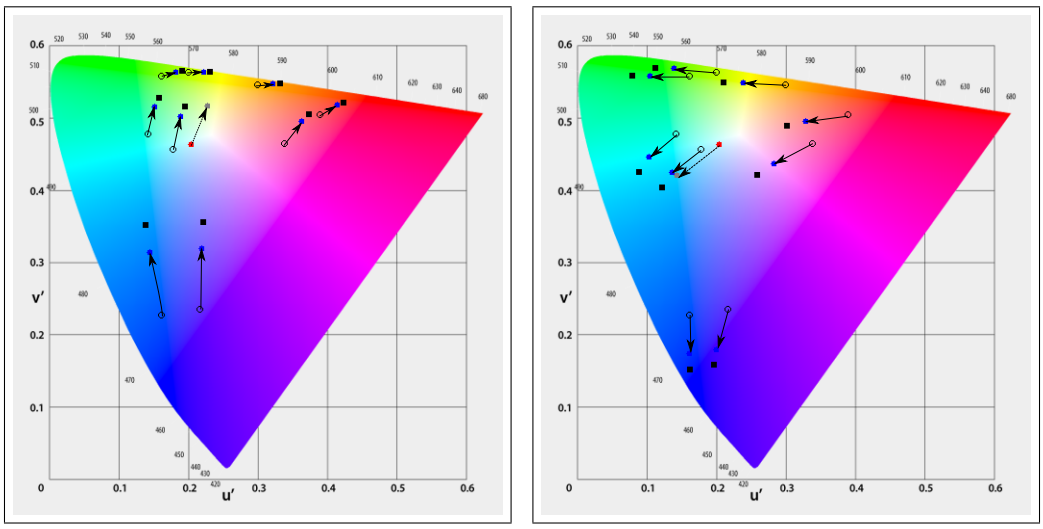

Figure 5.8: Color changes predicted by Fairchild's model and von Kries model on the CIE $u'v'$ diagram. Red dots: original illuminant. Gray dots: new illuminant. Black dots: predictions of Fairchild's model. Blue dots: predictions of von Kries model.

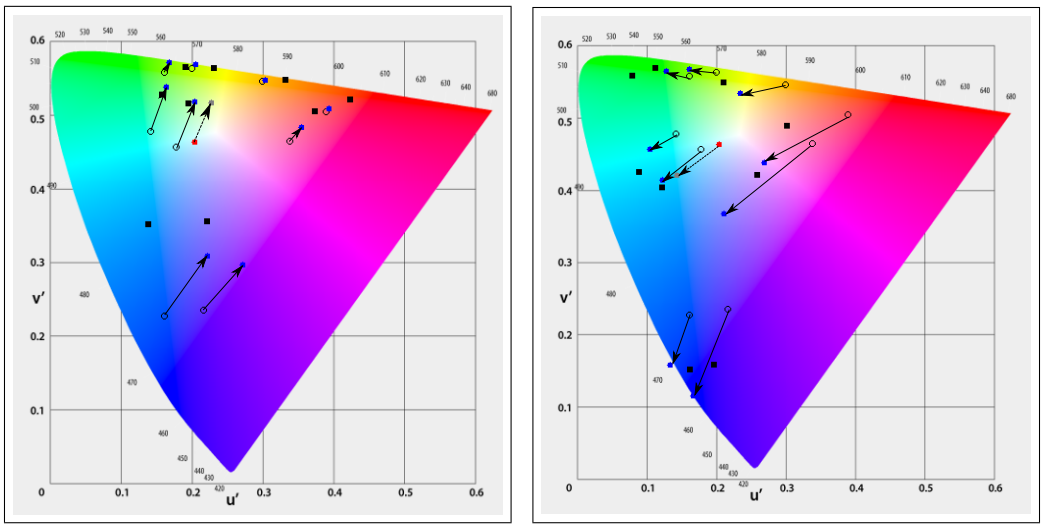

Figure 5.9: Color changes predicted by CIELAB and von Kries model on the CIE $u'v'$ diagram. Red dots: original illuminant. Gray dots: new illuminant. Black dots: predictions of CIELAB. Blue dots: predictions of von Kries model.

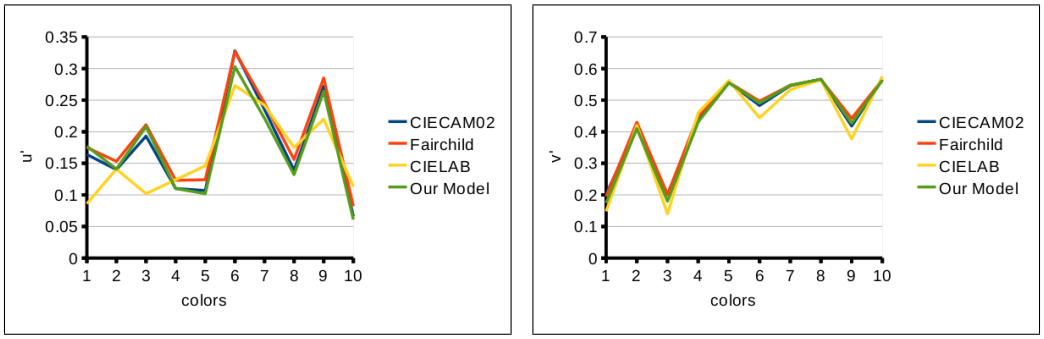

(a) Plots of $u'v'$ values for illuminant changes from E to A.

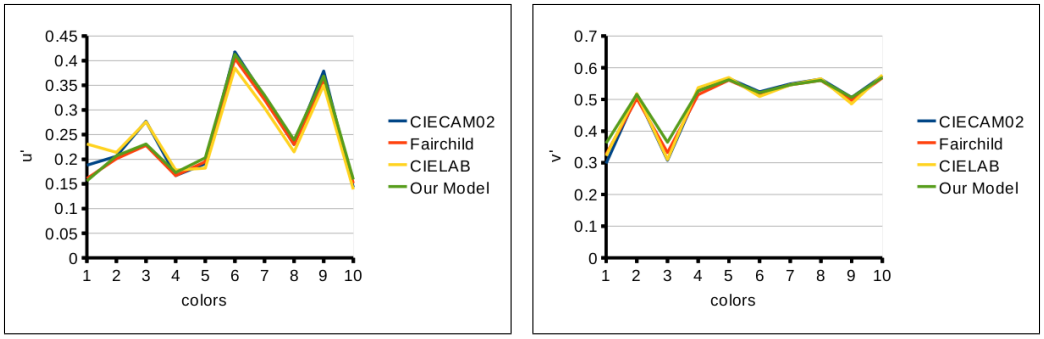

(b) Plots of $u'v'$ values for illuminant changes from E to cyan light.

Figure 5.10: Plots of $u'v'$ values for predicted color changes.

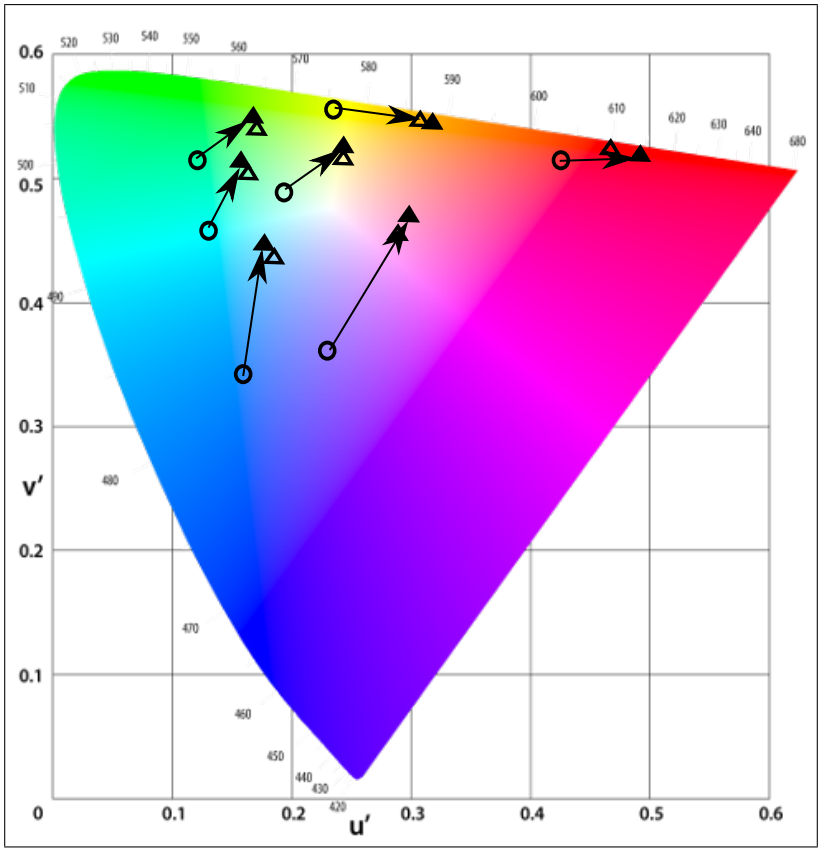

Figure 5.11: Predictions of corresponding-colors data using the von Kries model for illuminants changing from simulated daylight ($D65$) to incandescent light (A). Open triangles: visual data. Filled triangles: model predictions.

Figure 5.12: Test images under illuminant E.

Figure 5.13: Adjusted images for displaying under illuminant A. Top left: CIECAM02. Top right: Fairchild's. Bottom left: CIELAB. Bottom right: von Kries.

Figure 5.14: Adjusted images for displaying under illuminant A. Top left: CIECAM02. Top right: Fairchild's. Bottom left: CIELAB. Bottom right: von Kries.

Figure 5.15: Adjusted images for displaying under cyan illuminant. Top left: CIECAM02. Top right: Fairchild's. Bottom left: CIELAB. Bottom right: von Kries.

Figure 5.16: Adjusted images for displaying under cyan illuminant. Top left: CIECAM02. Top right: Fairchild's. Bottom left: CIELAB. Bottom right: von Kries.

Chapter 6

Conclusions

6.1 Contributions

This thesis presents research that examined fluorescence and adaptation in color images. It makes the following contributions:

- It provides a model of fluorescence and of the difference in color appearance between fluorescence and reflectance under arbitrary illuminants.
- It shows how to separate the fluorescent and reflective components of an image using independent component analysis. The separation provides an improved method for relighting images under arbitrary illuminants.
- It proposes a practical model for adaptive displays based on a von Kries model of chromatic adaptation. The model takes into account the mixed adaptation that occurs when viewers observe images on self-luminous displays. Examples show that the model is simple, efficient, and produces results comparable to existing models.

6.2 Limitations and Future Work

Fluorescence in color images

Using independent component analysis (ICA) for separating reflective and fluorescent components of an image is novel in color imaging. Its limitations remain to be explored. First, ICA assumes that there are no correlations between the spatial distributions of the reflective and fluorescent components. Some statistical evidence should be obtained to support or disprove this assumption. Second, ICA is used to separate the fluorescent and reflective components because the required separation strongly resembles the work of Farid and Adelson [14]. The thesis presents results for applying ICA to the reflectance-fluorescence separation problem, but omits a mathematical model of the separation process. In future work, I will work on a formal model for the separation problem.

The originality of the work, on the other hand, provides insights useful in other research areas. My study shows that the intensity of fluorescence varies with the intensity of illumination. This finding may be useful in color constancy for discovering methods that extract information about illuminants from the intensity of the observed fluorescence. The constant chromaticity property of fluorescent materials should make them ideal colorants for products that require unchanging color when the illumination varies, such as color-coded labels and barcodes.

Adaptation in color images and adaptive displays

The model for adaptive displays proposed in this thesis is based on several assumptions. First, the displayed image is assumed to have a single illuminant in the scene portrayed. This assumption restricts the application of the model, because many images contain multiple scene illuminants. Second, while the model considers the color of the illuminants in the scene and the viewing environment, it does not take into account other factors such as viewing angles, brightness of the surround, contrast of lighting in the viewing environment and so on. Third, like all color appearance models, the proposed model accounts only for post-receptoral processes. Pre-receptoral changes to color appearance, such as metamerism, are not included in the model. Moreover, issues of display calibration, such as gamma correction, are overlooked

during derivation of the model. Since the model is designed to be practical, it will be interesting to build an adaptive display based on the model, so as to perform user studies and psychophysical evaluations.

APPENDICES

Appendix A

Einstein Notation

Einstein notation or Einstein summation convention is very powerful and useful in linear algebra and physics. In Einstein notation, when an index variable appears twice in a single term, once as superscript and once as subscript, it implies that we are summing over all of its possible values. For example in three dimensions, $y = c_i x^i$ means

$$y = \sum_i c_i x^i = \sum_{i=1}^{3} c_i x^i = c_1 x^1 + c_2 x^2 + c_3 x^3.$$

The inner product of a row vector v and a column vector u is a scalar $v_i u^i$.

For a matrix A, the element for the m^{th} row and n^{th} column is A_n^m. The result of matrix A multiplied by a column vector v, Av, becomes $A_j^i v^j$.

Matrix multiplication can be represented as

$$C_k^i = A_j^i B_k^j$$

which is the equivalent to the conventional (less compact) notation

$$C_{ik} = (AB)_{jk} = \sum_{j=1}^{N} A_{ij} B_{jk}.$$

The Kronecker delta can be written as δ_j^i, so δ_j^i is 1 if $i = j$ and 0 otherwise.

Appendix B

Tristimulus Values

Suppose the spectral power distribution (the intensity and distribution of the spectrum) for a color at point x over a range of wavelength λ is $E(\lambda)$. Then its tristimulus values are defined as

$$X = \int_0^\infty \bar{x}(\lambda) E(\lambda)\, \mathrm{d}\lambda,$$
$$Y = \int_0^\infty \bar{y}(\lambda) E(\lambda)\, \mathrm{d}\lambda,$$
$$Z = \int_0^\infty \bar{z}(\lambda) E(\lambda)\, \mathrm{d}\lambda.$$

where $\bar{x}(\lambda)$, $\bar{y}(\lambda)$, $\bar{z}(\lambda)$ are the CIE color matching functions. Usually, the range of λ is taken to be the visible spectrum, $[380\,\mathrm{nm}, 720\,\mathrm{nm}]$, rather than $(0, \infty)$.

In Einstein notation (Appendix A), the tristimulus values of the color at point x can be represented in a compact way as

$$\mathbf{X}^i(x) = \bar{x}^i_\lambda E^\lambda(x),$$

where $i = \{X, Y, Z\}$.

Appendix C

Dimension Analysis for Solving New Scene Illumination

In Einstein notation, the equation we are trying to solve is

$$\alpha_s^r M_j^s \hat{x}_\lambda^j R_\mu^\lambda(x) \underset{\sim}{I}^\mu = M_i^r \hat{x}_\lambda^i R_\mu^\lambda(x) I^\mu.$$

In practice, the matrices have the form

$$\begin{bmatrix} *_{11} & 0 & 0 \\ 0 & *_{22} & 0 \\ 0 & 0 & *_{33} \end{bmatrix} \begin{bmatrix} *_{11} & *_{12} & *_{13} \\ *_{21} & *_{22} & *_{23} \\ *_{31} & *_{32} & *_{33} \end{bmatrix} \begin{bmatrix} *_{11} & *_{12} & \cdots & *_{1N} \\ *_{21} & *_{22} & \cdots & *_{2N} \\ *_{31} & *_{32} & \cdots & *_{3N} \end{bmatrix} \begin{bmatrix} *_{11} & 0 & \cdots & 0 \\ 0 & *_{22} & \cdots & 0 \\ \vdots & & \ddots & \vdots \\ 0 & 0 & \cdots & *_{NN} \end{bmatrix} \begin{bmatrix} *_1 \\ *_2 \\ \vdots \\ *_N \end{bmatrix}$$

$$= \begin{bmatrix} *_{11} & *_{12} & *_{13} \\ *_{21} & *_{22} & *_{23} \\ *_{31} & *_{32} & *_{33} \end{bmatrix} \begin{bmatrix} *_{11} & *_{12} & \cdots & *_{1N} \\ *_{21} & *_{22} & \cdots & *_{2N} \\ *_{31} & *_{32} & \cdots & *_{3N} \end{bmatrix} \begin{bmatrix} *_{11} & 0 & \cdots & 0 \\ 0 & *_{22} & \cdots & 0 \\ \vdots & & \ddots & \cdots \\ 0 & 0 & \cdots & *_{NN} \end{bmatrix} \begin{bmatrix} *_1 \\ *_2 \\ \vdots \\ *_N \end{bmatrix},$$

where N is the number of samples for wavelength λ and μ. The subscripts and superscripts representing dimensions are omitted for simplicity.

Simplify using $c_\lambda^r = M_i^r \hat{x}_\lambda^i$,

$$
\begin{aligned}
LHS &= \begin{bmatrix} *_{11} & 0 & 0 \\ 0 & *_{22} & 0 \\ 0 & 0 & *_{33} \end{bmatrix} \begin{bmatrix} *_{11} & *_{12} & \cdots & *_{1N} \\ *_{21} & *_{22} & \cdots & *_{2N} \\ *_{31} & *_{32} & \cdots & *_{3N} \end{bmatrix} \begin{bmatrix} *_{11} & 0 & \cdots & 0 \\ 0 & *_{22} & \cdots & 0 \\ \vdots & & \ddots & \cdots \\ 0 & 0 & \cdots & *_{NN} \end{bmatrix} \begin{bmatrix} *_1 \\ *_2 \\ .. \\ *_N \end{bmatrix} \\
&= \begin{bmatrix} \alpha \end{bmatrix} \begin{bmatrix} c \end{bmatrix} \begin{bmatrix} R \end{bmatrix} \begin{bmatrix} \underset{\sim}{I} \end{bmatrix} \\
RHS &= \begin{bmatrix} *_{11} & *_{12} & \cdots & *_{1N} \\ *_{21} & *_{22} & \cdots & *_{2N} \\ *_{31} & *_{32} & \cdots & *_{3N} \end{bmatrix} \begin{bmatrix} *_{11} & 0 & \cdots & 0 \\ 0 & *_{22} & \cdots & 0 \\ \vdots & & \ddots & \cdots \\ 0 & 0 & \cdots & *_{NN} \end{bmatrix} \begin{bmatrix} *_1 \\ *_2 \\ \vdots \\ *_N \end{bmatrix} \\
&= \begin{bmatrix} c \end{bmatrix} \begin{bmatrix} R \end{bmatrix} \begin{bmatrix} I \end{bmatrix}
\end{aligned}
$$

Decompose the reflectance as

$$\begin{bmatrix} R \end{bmatrix} = n_1 \begin{bmatrix} R_1 \end{bmatrix} + n_2 \begin{bmatrix} R_2 \end{bmatrix} + n_3 \begin{bmatrix} R_3 \end{bmatrix},$$

where n_i is the i^{th} coefficients. R_i are the basis functions for illuminant.

Similarly, the illuminant can be decomposed as

$$\begin{bmatrix} I \end{bmatrix} = m_1 \begin{bmatrix} I_1 \end{bmatrix} + m_2 \begin{bmatrix} I_2 \end{bmatrix} + m_3 \begin{bmatrix} I_3 \end{bmatrix}, \quad \begin{bmatrix} \underset{\sim}{I} \end{bmatrix} = \underset{\sim}{m}_1 \begin{bmatrix} I_1 \end{bmatrix} + \underset{\sim}{m}_2 \begin{bmatrix} I_2 \end{bmatrix} + \underset{\sim}{m}_3 \begin{bmatrix} I_3 \end{bmatrix},$$

where m_i and $\underset{\sim}{m}_i$ are the i^{th} coefficients. I_i are the basis functions for illuminants.

Substitute in the decompositions, we have

$$
\begin{aligned}
LHS &= \begin{bmatrix} \alpha \end{bmatrix} \begin{bmatrix} c \end{bmatrix} \left(n_1 \begin{bmatrix} R_1 \end{bmatrix} + n_2 \begin{bmatrix} R_2 \end{bmatrix} + n_3 \begin{bmatrix} R_3 \end{bmatrix} \right) \left(\underset{\sim}{m}_1 \begin{bmatrix} I_1 \end{bmatrix} + \underset{\sim}{m}_2 \begin{bmatrix} I_2 \end{bmatrix} + \underset{\sim}{m}_3 \begin{bmatrix} I_3 \end{bmatrix} \right) \\
&= \begin{bmatrix} \alpha \end{bmatrix} \begin{bmatrix} c \end{bmatrix} \left(n_1 \underset{\sim}{m}_1 \begin{bmatrix} R_1 \end{bmatrix} \begin{bmatrix} I_1 \end{bmatrix} + n_1 \underset{\sim}{m}_2 \begin{bmatrix} R_1 \end{bmatrix} \begin{bmatrix} I_2 \end{bmatrix} + \cdots + n_3 \underset{\sim}{m}_3 \begin{bmatrix} R_3 \end{bmatrix} \begin{bmatrix} I_3 \end{bmatrix} \right)
\end{aligned}
$$

$$
\begin{aligned}
RHS &= \begin{bmatrix} c \end{bmatrix} \left(n_1 \begin{bmatrix} R_1 \end{bmatrix} + n_2 \begin{bmatrix} R_2 \end{bmatrix} + n_3 \begin{bmatrix} R_3 \end{bmatrix} \right) \left(m_1 \begin{bmatrix} I_1 \end{bmatrix} + m_2 \begin{bmatrix} I_2 \end{bmatrix} + m_3 \begin{bmatrix} I_3 \end{bmatrix} \right) \\
&= \begin{bmatrix} c \end{bmatrix} \left(n_1 m_1 \begin{bmatrix} R_1 \end{bmatrix} \begin{bmatrix} I_1 \end{bmatrix} + n_1 m_2 \begin{bmatrix} R_1 \end{bmatrix} \begin{bmatrix} I_2 \end{bmatrix} + \cdots + n_3 m_3 \begin{bmatrix} R_3 \end{bmatrix} \begin{bmatrix} I_3 \end{bmatrix} \right)
\end{aligned}
$$

Define a "3×3" block matrix (a matrix of matrices) Q that has the form

$$Q = \begin{bmatrix} [] & [] & [] \\ [] & [] & [] \\ [] & [] & [] \end{bmatrix},$$

where each block is an $N \times 1$ matrix. Q_{ij} represents the spectral power distribution of the i^{th} reflectance basis, R_i with dimension $N \times N$, interacting with the j^{th} illuminant basis, I_j with dimension $N \times 1$. Q can be pre-computed since the basis functions are all known beforehand.

Now the original equation C.1 has the matrix form

$$\begin{bmatrix} \alpha \end{bmatrix}\begin{bmatrix} c \end{bmatrix}\begin{bmatrix} n_1 & n_2 & n_3 \end{bmatrix}\begin{bmatrix} Q \end{bmatrix}\begin{bmatrix} \mathfrak{m}_1 \\ \mathfrak{m}_2 \\ \mathfrak{m}_3 \end{bmatrix} = \begin{bmatrix} c \end{bmatrix}\begin{bmatrix} n_1 & n_2 & n_3 \end{bmatrix}\begin{bmatrix} Q \end{bmatrix}\begin{bmatrix} m_1 \\ m_2 \\ m_3 \end{bmatrix}.$$

Suppose we have a set of values for $\begin{bmatrix} n_1 & n_2 & n_3 \end{bmatrix}$. Then we can compute the product of $\begin{bmatrix} c \end{bmatrix}\begin{bmatrix} n_1 & n_2 & n_3 \end{bmatrix}\begin{bmatrix} Q \end{bmatrix}$. The dimension of the product is a 3×3 matrix because $\begin{bmatrix} c \end{bmatrix}$ is $3 \times N$, $\begin{bmatrix} n_1 & n_2 & n_3 \end{bmatrix}$ is 1×3, and $\begin{bmatrix} Q \end{bmatrix}$ is 3×3 with each entry $N \times 1$. Let Ψ be the 3×3 matrix, then

$$\begin{bmatrix} \alpha \end{bmatrix}\begin{bmatrix} \Psi \end{bmatrix}\begin{bmatrix} \mathfrak{m}_1 \\ \mathfrak{m}_2 \\ \mathfrak{m}_3 \end{bmatrix} = \begin{bmatrix} \Psi \end{bmatrix}\begin{bmatrix} m_1 \\ m_2 \\ m_3 \end{bmatrix},$$

$$\begin{bmatrix} \mathfrak{m}_1 \\ \mathfrak{m}_2 \\ \mathfrak{m}_3 \end{bmatrix} = \begin{bmatrix} \Psi \end{bmatrix}^{-1}\begin{bmatrix} \alpha \end{bmatrix}^{-1}\begin{bmatrix} \Psi \end{bmatrix}\begin{bmatrix} m_1 \\ m_2 \\ m_3 \end{bmatrix}.$$

Appendix D

Color Appearance Models

D.1 CIELAB

User Input: (X_i, Y_i, Z_i), tristimulus values of the testing patch.

Input Parameters:

- $(X_{w,\,scene}, Y_{w,\,scene}, Z_{w,\,scene})$, tristimulus values of the white point of the scene illuminant.
- $(X_{w,\,view}, Y_{w,\,view}, Z_{w,\,view})$, tristimulus values of the white point of the view illuminant.

Onput: (X_o, Y_o, Z_o), tristimulus values of the test patch after compensation.

Forward Model:

STEP 1: Normalize the tristimulus values of the white point of the scene illuminant.

$$\begin{aligned} X_{n,\,scene} &= \frac{X_{w,\,scene}}{\sqrt{X_{w,\,scene}^2 + Y_{w,\,scene}^2 + Z_{w,\,scene}^2}} \\ Y_{n,\,scene} &= \frac{Y_{w,\,scene}}{\sqrt{X_{w,\,scene}^2 + Y_{w,\,scene}^2 + Z_{w,\,scene}^2}} \\ Z_{n,\,scene} &= \frac{Z_{w,\,scene}}{\sqrt{X_{w,\,scene}^2 + Y_{w,\,scene}^2 + Z_{w,\,scene}^2}} \end{aligned}$$

STEP 2: Compute CIELAB values.

$$\begin{aligned} L &= 116 f(Y_i/Y_{n,\,scene}) - 16 \\ a &= 500[f(X_i/X_{n,\,scene}) - f(Y_i/Y_{n,\,scene})] \\ b &= 200[f(Y_i/Y_{n,\,scene}) - f(Z_i/Z_{n,\,scene})], \end{aligned}$$

where

$$f(t) = \begin{cases} t^{1/3} & \text{if} t > (\frac{6}{29})^3 \\ \frac{1}{3}(\frac{29}{6})^2 t + \frac{4}{29} & \text{otherwise} \end{cases}.$$

Reverse Model:

Compute the tristimulus values (X_o, Y_o, Z_o) of the output.

$$\begin{aligned} X_o &= X_{n,\,view} f^{-1}\left(\frac{L+16}{116} + \frac{a}{500}\right) \\ Y_o &= Y_{n,\,view} f^{-1}\left(\frac{L+16}{116}\right) \\ Z_o &= Z_{n,\,view} f^{-1}\left(\frac{L+16}{116} - \frac{b}{200}\right) \end{aligned}$$

where

$$f^{-1}(t) = \begin{cases} t^3 & \text{if} t > \frac{6}{29} \\ 3(\frac{6}{29})^2(t - \frac{4}{29}) & \text{otherwise} \end{cases}.$$

D.2 CIECAM02

User Input: (X_i, Y_i, Z_i), tristimulus values of the testing patch.

Input/Scene Parameters:

- $(X_{w,\,scene}, Y_{w,\,scene}, Z_{w,\,scene})$, relative tristimulus values of the white point of the scene illuminant. $Y_{w,\,scene}$ is always set to 100.
- $(X_{w,\,view}, Y_{w,\,view}, Z_{w,\,view})$, relative tristimulus values of the white point of the scene illuminant. $Y_{w,\,scene}$ is always set to 100.

- Y_b, relative luminance of the background. Assume “grey world". 20% of Y_w so it is always set to 20.
- L_A, adapting field luminance. Always set to $64cd/m^2$ in my model because it is the most commonly used value. I experimented with a few values, but none seemed to have significant impact on the results.
- c, F, N_c, relative luminance level of the surround. All set to “average" in my model for now. $c = 0.69, F = 1.0, N_c = 1.0$.

Onput: (X_o, Y_o, Z_o), tristimulus values of the test patch after compensation.

Step 1: Compute intermediate variables used when calculating perceptual attributes.

$$\begin{aligned} k &= \frac{1}{5L_A + 1} \\ F_L &= 0.2k^4(5L_A) + 0.1(1 - k^4)^2(5L_A) \\ n &= \frac{Y_b}{Y_w} \\ N_{cb} &= N_{bb} = 0.725(\frac{1}{n})^{\frac{1}{2}} \\ z &= 1.48 + \sqrt{n} \end{aligned}$$

Step 2: Chromatic adaptation. Convert tristimulus values to CAT02 (chromatic adaptation transform) space. For CAT02 space, $X_w = Y_w = Z_w = 100.0$; *i.e.*, “equal-energy".

$$\begin{bmatrix} R \\ G \\ B \end{bmatrix} = M_{CAT02} \begin{bmatrix} X_i \\ Y_i \\ Z_i \end{bmatrix}, \quad \begin{bmatrix} R_w \\ G_w \\ B_w \end{bmatrix} = M_{CAT02} \begin{bmatrix} X_{w,\,scene} \\ Y_{w,\,scene} \\ Z_{w,\,scene} \end{bmatrix},$$

where

$$M_{CAT02} = \begin{bmatrix} 0.7328 & 0.4286 & -0.1624 \\ -0.7036 & 1.6975 & 0.0061 \\ 0.0030 & 0.0136 & 0.9834 \end{bmatrix}.$$

Step 3: Determine degree of adaptation.

$$D = F[1 - (\frac{1}{3.6}e^{\frac{-L_A - 42}{92}})]$$

For my model, D is suggested to be set to 1.0 for self-illuminated displays.

Step 4: Chromatic adaptation transform [1].

$$\begin{aligned}
R_c &= [(\frac{Y_w D}{R_w}) + (1.0 - D)]R \\
G_c &= [(\frac{Y_w D}{G_w}) + (1.0 - D)]G \\
B_c &= [(\frac{Y_w D}{B_w}) + (1.0 - D)]B \\
R_{wc} &= [(\frac{Y_w D}{R_w}) + (1.0 - D)]R_w \\
G_{wc} &= [(\frac{Y_w D}{G_w}) + (1.0 - D)]G_w \\
B_{wc} &= [(\frac{Y_w D}{B_w}) + (1.0 - D)]B_w
\end{aligned}$$

Step 5: Convert to Hunt-Pointer-Estevez space.

$$\begin{bmatrix} R'_a \\ G'_a \\ B'_a \end{bmatrix} = M_H M_{CAT02}^{-1} \begin{bmatrix} R_c \\ G_c \\ B_c \end{bmatrix}, \quad \begin{bmatrix} R'_{wa} \\ G'_{wa} \\ B'_{wa} \end{bmatrix} = M_H M_{CAT02}^{-1} \begin{bmatrix} R_{wc} \\ G_{wc} \\ B_{wc} \end{bmatrix},$$

where

$$M_H M_{CAT02}^{-1} = \begin{bmatrix} 0.7410 & 0.2180 & 0.0410 \\ -0.2854 & 0.6242 & 0.0904 \\ -0.0096 & -0.0057 & 1.0153 \end{bmatrix}.$$

[1] The technical report from CIE does not explicitly give the equations for computing R_{wc}, R'_{wa}, A_w, *etc.*. I derived the calculations myself from R_c, R'_c, A, *etc.*.

STEP 6: Non-linear response compression. “Essential for working in perceptual space".

$$
\begin{aligned}
R'_a &= [\frac{400(\frac{F_L R'_a}{100})^{0.42}}{27.13+(\frac{F_L R'_a}{100})^{0.42}}]+0.1 \\
G'_a &= [\frac{400(\frac{F_L G'_a}{100})^{0.42}}{27.13+(\frac{F_L G'_a}{100})^{0.42}}]+0.1 \\
B'_a &= [\frac{400(\frac{F_L B'_a}{100})^{0.42}}{27.13+(\frac{F_L B'_a}{100})^{0.42}}]+0.1 \\
R'_{wa} &= [\frac{400(\frac{F_L R'_{wa}}{100})^{0.42}}{27.13+(\frac{F_L R'_{wa}}{100})^{0.42}}]+0.1 \\
G'_{wa} &= [\frac{400(\frac{F_L G'_{wa}}{100})^{0.42}}{27.13+(\frac{F_L G'_{wa}}{100})^{0.42}}]+0.1 \\
B'_{wa} &= [\frac{400(\frac{F_L B'_{wa}}{100})^{0.42}}{27.13+(\frac{F_L B'_{wa}}{100})^{0.42}}]+0.1
\end{aligned}
$$

If any of the values of $R'_a, G'_a, B'_a, R'_{wa}, G'_{wa}, B'_{wa}$ are negative, their absolute values are used, and then the quotient is multiplied by negative 1 before adding to 0.1.

STEP 7: Calculate perceptual attributes. The most important values are J(Lightness), C(Chroma) and h(Hue).

$$
\begin{aligned}
A &= (2.0R'_a + G'_a + 0.05B'_a - 0.305)N_{bb} \\
A_w &= (2.0R'_{wa} + G'_{wa} + 0.05B'_{wa} - 0.305)N_{bb} \\
J &= 100(\frac{A}{A_w})^{cz} \\
a &= R'_a - \frac{12G'_a}{11} + \frac{B'_a}{11},\ b = (\frac{1}{9})(R'_a + G'_a - 2B'_a) \\
h &= tan^{-1}(\frac{b}{a}), 0 \leq h \leq 360 \\
e &= 0.25[cos(\frac{h\pi}{180}+2)+3.8] \\
t &= \frac{(\frac{50{,}000}{13})N_c N_{cb} e(a^2+b^2)^{0.5}}{R'_a + G'_a + (\frac{21}{20})B'_a} \\
C &= t^{0.9}(\frac{J}{100})^{0.5}(1.64-0.29^n)^{0.73}
\end{aligned}
$$

If two color patches have the same $[J, C, h]$, we perceive them as having the same color, regardless of surrounding environment.

Reverse Model:

STEP 1: Compute intermediate variables $k, F_L, n, N_{bb}, N_{cb}, z$. Same equations from the forward model are used. The input/scene parameters are replaced by the input/view parameters.

STEP 2 - 6: Same as forward model, except that only reference white is considered and all the scene parameters are replaced by view parameters.

STEP 7: Compute temporary variables $t, e_t, A, p_1, p_2, p_3, hr, a, b$.

$$\begin{aligned} t &= \left(\frac{C}{\sqrt{\frac{J}{100}}(1.64 - 0.29^n)^{0.73}}\right)^{\frac{1}{0.9}} \\ e_t &= \frac{1}{4}(cos(h(\frac{\pi}{180}) + 2) + 3.8) \\ p_1 &= \frac{(50000/13)N_c N_{cb} e_t}{t} \\ p_2 &= (\frac{A}{N_{bb}}) + 0.305 \\ hr &= h(\frac{\pi}{180}) \end{aligned}$$

if $|sin(hr)| \geq |cos(hr)|$,

$$p_3 = \frac{p_1}{sin(hr)}$$

$$b = \frac{p_2(2.0 + (21/20))(460/1403)}{p_3 + (2.0 + (21/20))(220/1403)[cos(hr)/sin(hr)] - (27/1403) + (21/20)(6300/1403)}$$

$$a = b[cos(hr)/sin(hr)]$$

else

$$p_3 = \frac{p_1}{cos(hr)}$$

$$a = \frac{p_2(2.0 + (21/20))(460/1403)}{p_3 + (2.0 + (21/20))(220/1403) - [(27/1403) - (21/20)(6300/1403)][sin(hr)/cos(hr)]}$$

$$b = a[sin(hr)/cos(hr)]$$

STEP 8: Compute R'_a, G'_a, B'_a.

$$\begin{aligned} R'_a &= (460/1403)p_2 + (451/1403)a + (288/1403)b \\ G'_a &= (460/1403)p_2 - (891/1403)a - (261/1403)b \\ B'_a &= (460/1403)p_2 - (220/1403)a - (6300/1403)b \end{aligned}$$

STEP 9: Compute R', G', B'.

$$\begin{aligned} R' &= (\frac{100}{F_L})(\frac{27.31|R'_a - 0.1|}{400 - |R'_a - 0.1|})^{\frac{1}{0.42}} \\ G' &= (\frac{100}{F_L})(\frac{27.31|G'_a - 0.1|}{400 - |G'_a - 0.1|})^{\frac{1}{0.42}} \\ B' &= (\frac{100}{F_L})(\frac{27.31|B'_a - 0.1|}{400 - |B'_a - 0.1|})^{\frac{1}{0.42}} \end{aligned}$$

If any of the values of $(R'_a - 0.1)$, $(G'_a - 0.1)$ or $(B'_a - 0.1)$ are negative, the corresponding R', G' or B' will be made negative.

STEP 10: Compute R_c, G_c, B_c.

$$\begin{bmatrix} R_c \\ G_c \\ B_c \end{bmatrix} = M_{CAT02}M_H^{-1} \begin{bmatrix} R' \\ G' \\ B' \end{bmatrix},$$

where

$$M_{CAT02}M_H^{-1} = \begin{bmatrix} 1.559 & -0.5447 & -0.01448 \\ -0.7143 & 1.8503 & -0.1360 \\ 0.01078 & 0.00522 & 0.9840 \end{bmatrix}.$$

STEP 11: Compute R, G, B.

$$\begin{aligned} R &= \frac{R_c}{[(\frac{Y_w D}{Rw}) + (1.0 - D)]} \\ G &= \frac{G_c}{[(\frac{Y_w D}{Gw}) + (1.0 - D)]} \\ B &= \frac{B_c}{[(\frac{Y_w D}{Bw}) + (1.0 - D)]} \end{aligned}$$

Step 12: Compute X_o, Y_o, Z_o.

$$\begin{bmatrix} X_o \\ Y_o \\ Z_o \end{bmatrix} = M_{CAT02}^{-1} \begin{bmatrix} R \\ G \\ B \end{bmatrix},$$

where

$$M_{CAT02}^{-1} = \begin{bmatrix} 1.096124 & -0.278869 & 0.182745 \\ 0.454396 & 0.473533 & 0.072098 \\ -0.009628 & -0.005698 & 1.015326 \end{bmatrix}.$$

D.3 Fairchild's Model

User Input: (X_i, Y_i, Z_i), tristimulus values of the test patch.

Input Parameters:

- $(X_{w,\,scene}, Y_{w,\,scene}, Z_{w,\,scene})$, tristimulus values of the white point of the scene illuminant.
- $Y_{w,\,scene}$ is always set to 100.0 (normalized).
- $(X_{w,\,view}, Y_{w,\,view}, Z_{w,\,view})$, tristimulus values of the white point of the view illuminant.
- $Y_{w,\,view}$ is always set to 100.0.

Onput: (X_o, Y_o, Z_o), tristimulus values of the test patch after compensation.

Forward Model:

Step 1: Compute the initial cone response (L, M, S) to the input.

$$\begin{bmatrix} L \\ M \\ S \end{bmatrix} = M \begin{bmatrix} X_i \\ Y_i \\ Z_i \end{bmatrix},$$

where

$$M = \begin{bmatrix} 0.400 & 0.708 & -0.081 \\ -0.226 & 1.165 & 0.046 \\ 0.000 & 0.000 & 0.918 \end{bmatrix}.$$

STEP 2: Compute the maximum cone response $(L_{w,\,scene}, M_{w,\,scene}, S_{w,\,scene})$ to the scene illuminant. *i.e.,* the cone response to the white point of the scene illuminant, as well as the maximum cone response $(L_{w,\,E}, M_{w,\,E}, S_{w,\,E})$ to the equal-energy illuminant.

$$\begin{bmatrix} L_w \\ M_w \\ S_w \end{bmatrix} = M \begin{bmatrix} X_{w,\,scene} \\ Y_{w,\,scene} \\ Z_{w,\,scene} \end{bmatrix}, \quad \begin{bmatrix} L_{w,\,E} \\ M_{w,\,E} \\ S_{w,\,E} \end{bmatrix} = M \begin{bmatrix} X_{w,\,E} \\ Y_{w,\,E} \\ Z_{w,\,E} \end{bmatrix},$$

$$X_{w,\,E} = Y_{w,\,E} = Z_{w,\,E} = 100.0$$

STEP 3: Compute the post-adaptation cone response (L_a, M_a, S_a) to the input. Fairchild's Model takes into consideration of how adapting luminance level may affect the state of adaptation (incomplete vs complete).

STEP 3.1: Compute the intermediate post-adaptation cone response (L_i, M_i, S_i) to the input.

$$\begin{bmatrix} L_i \\ M_i \\ S_i \end{bmatrix} = A \begin{bmatrix} L \\ M \\ S \end{bmatrix},$$

where

$$A = \begin{bmatrix} a_L & 0 & 0 \\ 0 & a_M & 0 \\ 0 & 0 & a_S \end{bmatrix} = \begin{bmatrix} p_L / L_{w,\,scene} & 0 & 0 \\ 0 & p_M / M_{w,\,scene} & 0 \\ 0 & 0 & p_S / S_{w,\,scene} \end{bmatrix},$$

$$p_L = \frac{1 + Y_{n,\,scene}^{1/3} + m_e}{1 + Y_{n,\,scene}^{1/3} + (1/m_e)},\ m_e = \frac{3(L_{w,\,scene}/L_{w,\,E})}{(L_{w,\,scene}/L_{w,\,E}) + (M_{w,\,scene}/M_{w,\,E}) + (S_{w,\,scene}/S_{w,\,E})},$$

$$p_M = \frac{1 + Y_{n,\,scene}^{1/3} + m_e}{1 + Y_{n,\,scene}^{1/3} + (1/m_e)},\ m_e = \frac{3(M_{w,\,scene}/M_{w,\,E})}{(L_{w,\,scene}/L_{w,\,E}) + (M_{w,\,scene}/M_{w,\,E}) + (S_{w,\,scene}/S_{w,\,E})},$$

$$p_S = \frac{1 + Y_{n,\,scene}^{1/3} + m_e}{1 + Y_{n,\,scene}^{1/3} + (1/m_e)},\ m_e = \frac{3(S_{w,\,scene}/S_{w,\,E})}{(L_{w,\,scene}/L_{w,\,E}) + (M_{w,\,scene}/M_{w,\,E}) + (S_{w,\,scene}/S_{w,\,E})}.$$

Notes:

- $Y_{n,\,scene}$ is the luminance of the adapting stimulus in cd/m^2. This is a variable we could experiment in simulations.

- When cognitive discount-illuminant occurs: $p_L = p_M = p_S = 1.0$.
- p_L, p_M and p_S depart from 1.0 as adaptation becomes incomplete.
- As adapting chromaticity moves further and further away from equal-energy illuminant E, adaptation becomes less complete.

STEP 3.2: Compute the post-adaptation cone response (L_a, M_a, S_a) to the input.

$$\begin{bmatrix} L_a \\ M_a \\ S_a \end{bmatrix} = C \begin{bmatrix} L_i \\ M_i \\ S_i \end{bmatrix},$$

where

$$C = \begin{bmatrix} 1 & c & c \\ c & 1 & c \\ c & c & 1 \end{bmatrix},\ c = 0.219 - 0.0784 log_{10}(Y_{n,\,scene})$$

Reverse Model:

STEP 1: Compute the maximum cone response $(L_{w,\,view}, M_{w,\,view}, S_{w,\,view})$ to the view illuminant. *i.e.,* the cone response to the white point of the view illuminant.

$$\begin{bmatrix} L_{w,\,view} \\ M_{w,\,view} \\ S_{w,\,view} \end{bmatrix} = M \begin{bmatrix} X_{w,\,view} \\ Y_{w,\,view} \\ Z_{w,\,view} \end{bmatrix},$$

STEP 2: From the post-adaptation cone response, compute initial cone response (L, M, S) to the output.

STEP 2.1: Compute the intermediate cone response (L_i, M_i, S_i) to the output.

$$\begin{bmatrix} L_i \\ M_i \\ S_i \end{bmatrix} = C'^{-1} \begin{bmatrix} L_a \\ M_a \\ S_a \end{bmatrix},$$

where

$$C' = \begin{bmatrix} 1 & c' & c' \\ c' & 1 & c' \\ c' & c' & 1 \end{bmatrix},\ c' = 0.219 - 0.0784 log_{10}(Y_{n,\,view})$$

Note: $Y_{n,\,scene}$ is the luminance of the adapting stimulus in cd/m^2. This is a variable we could experiment in simulations.

Step 2.2: Compute the initial cone response (L', M', S') to the output.

$$\begin{bmatrix} L' \\ M' \\ S' \end{bmatrix} = A'^{-1} \begin{bmatrix} L_i \\ M_i \\ S_i \end{bmatrix},$$

where

$$A' = \begin{bmatrix} a'_L & 0 & 0 \\ 0 & a'_M & 0 \\ 0 & 0 & a'_S \end{bmatrix} = \begin{bmatrix} p'_L / L_{w,\,view} & 0 & 0 \\ 0 & p'_M / M_{w,\,view} & 0 \\ 0 & 0 & p'_S / S_{w,\,view} \end{bmatrix},$$

$$p'_L = \frac{1 + Y_{n,\,view}^{1/3} + m_e}{1 + Y_{n,\,view}^{1/3} + (1/m_e)},\ m_e = \frac{3(L_{w,\,view}/L_{w,\,E})}{(L_{w,\,view}/L_{w,\,E}) + (M_{w,\,view}/M_{w,\,E}) + (S_{w,\,view}/S_{w,\,E})},$$

$$p'_M = \frac{1 + Y_{n,\,view}^{1/3} + m_e}{1 + Y_{n,\,view}^{1/3} + (1/m_e)},\ m_e = \frac{3(M_{w,\,view}/M_{w,\,E})}{(L_{w,\,view}/L_{w,\,E}) + (M_{w,\,view}/M_{w,\,E}) + (S_{w,\,view}/S_{w,\,E})},$$

$$p'_S = \frac{1 + Y_{n,\,view}^{1/3} + m_e}{1 + Y_{n,\,view}^{1/3} + (1/m_e)},\ m_e = \frac{3(S_{w,\,view}/S_{w,\,E})}{(L_{w,\,view}/L_{w,\,E}) + (M_{w,\,view}/M_{w,\,E}) + (S_{w,\,view}/S_{w,\,E})}.$$

Step 3: Compute the tristimulus values (X_o, Y_o, Z_o) of the output.

$$\begin{bmatrix} X_o \\ Y_o \\ Z_o \end{bmatrix} = M^{-1} \begin{bmatrix} L' \\ M' \\ S' \end{bmatrix}$$

Summary:

$$\begin{bmatrix} X_o \\ Y_o \\ Z_o \end{bmatrix} = M^{-1} \begin{bmatrix} a'_L & 0 & 0 \\ 0 & a'_M & 0 \\ 0 & 0 & a'_S \end{bmatrix}^{-1} C'^{-1} C \begin{bmatrix} a_L & 0 & 0 \\ 0 & a_M & 0 \\ 0 & 0 & a_S \end{bmatrix} M \begin{bmatrix} X_i \\ Y_i \\ Z_i \end{bmatrix}$$

or

$$C' \begin{bmatrix} a'_L & 0 & 0 \\ 0 & a'_M & 0 \\ 0 & 0 & a'_S \end{bmatrix} M \begin{bmatrix} X_o \\ Y_o \\ Z_o \end{bmatrix} = C \begin{bmatrix} a_L & 0 & 0 \\ 0 & a_M & 0 \\ 0 & 0 & a_S \end{bmatrix} M \begin{bmatrix} X_i \\ Y_i \\ Z_i \end{bmatrix}$$

D.4 von Kries Model

User Input: (X_i, Y_i, Z_i), tristimulus values of the test patch.

Input Parameters:

- $(X_{w,\,scene}, Y_{w,\,scene}, Z_{w,\,scene})$, tristimulus values of the white point of the scene illuminant.
- $Y_{w,\,scene}$ is always set to 100.0 (normalized).
- $(X_{w,\,view}, Y_{w,\,view}, Z_{w,\,view})$, tristimulus values of the white point of the view illuminant.
- $Y_{w,\,view}$ is always set to 100.0.

Onput: (X_o, Y_o, Z_o), tristimulus values of the test patch after compensation.

Forward Model:

Step 1: Compute the initial cone response (L, M, S) to the input.

$$\begin{bmatrix} L \\ M \\ S \end{bmatrix} = M \begin{bmatrix} X_i \\ Y_i \\ Z_i \end{bmatrix},$$

where

$$M = \begin{bmatrix} 0.400 & 0.708 & -0.081 \\ -0.226 & 1.165 & 0.046 \\ 0.000 & 0.000 & 0.918 \end{bmatrix}.$$

STEP 2: Compute the maximum cone response $(L_{w,\,scene}, M_{w,\,scene}, S_{w,\,scene})$ to the scene illuminant. *i.e.,* the cone response to the white point of the scene illuminant.

$$\begin{bmatrix} L_w \\ M_w \\ S_w \end{bmatrix} = M \begin{bmatrix} X_{w,\,scene} \\ Y_{w,\,scene} \\ Z_{w,\,scene} \end{bmatrix}$$

STEP 3: Compute the post-adaptation cone response (L_a, M_a, S_a) to the input. von Kries Model assumes that the process is linear.

$$\begin{bmatrix} L_a \\ M_a \\ S_a \end{bmatrix} = K \begin{bmatrix} L \\ M \\ S \end{bmatrix},$$

where

$$K = \begin{bmatrix} k_L & 0 & 0 \\ 0 & k_M & 0 \\ 0 & 0 & k_S \end{bmatrix} = \begin{bmatrix} 1/L_{w,\,scene} & 0 & 0 \\ 0 & 1/M_{w,\,scene} & 0 \\ 0 & 0 & 1/S_{w,\,scene} \end{bmatrix}.$$

Reverse Model:

STEP 1: Compute the maximum cone response $(L_{w,\,view}, M_{w,\,view}, S_{w,\,view})$ to the view illuminant. *i.e.,* the cone response to the white point of the view illuminant.

$$\begin{bmatrix} L_{w,\,view} \\ M_{w,\,view} \\ S_{w,\,view} \end{bmatrix} = M \begin{bmatrix} X_{w,\,view} \\ Y_{w,\,view} \\ Z_{w,\,view} \end{bmatrix},$$

STEP 2: Compute the initial cone response (L', M', S') from post-adaptation cone response.

$$\begin{bmatrix} L' \\ M' \\ S' \end{bmatrix} = K^{-1} \begin{bmatrix} L_a \\ M_a \\ S_a \end{bmatrix},$$

where

$$K = \begin{bmatrix} k_L & 0 & 0 \\ 0 & k_M & 0 \\ 0 & 0 & k_S \end{bmatrix} = \begin{bmatrix} 1/L_{w,\,view} & 0 & 0 \\ 0 & 1/M_{w,\,view} & 0 \\ 0 & 0 & 1/S_{w,\,view} \end{bmatrix}.$$

STEP 3: Compute the output tristimulus values (X_o, Y_o, Z_o) of the test patch after compensation.

$$\begin{bmatrix} X_o \\ Y_o \\ Z_o \end{bmatrix} = M^{-1} \begin{bmatrix} L' \\ M' \\ S' \end{bmatrix}.$$

Summary:

$$\begin{bmatrix} X_o \\ Y_o \\ Z_o \end{bmatrix} = M^{-1} \begin{bmatrix} k'_L & 0 & 0 \\ 0 & k'_M & 0 \\ 0 & 0 & k'_S \end{bmatrix}^{-1} \begin{bmatrix} k_L & 0 & 0 \\ 0 & k_M & 0 \\ 0 & 0 & k_S \end{bmatrix} M \begin{bmatrix} X_i \\ Y_i \\ Z_i \end{bmatrix}$$

or

$$\begin{bmatrix} k'_L & 0 & 0 \\ 0 & k'_M & 0 \\ 0 & 0 & k'_S \end{bmatrix} M \begin{bmatrix} X_o \\ Y_o \\ Z_o \end{bmatrix} = \begin{bmatrix} k_L & 0 & 0 \\ 0 & k_M & 0 \\ 0 & 0 & k_S \end{bmatrix} M \begin{bmatrix} X_i \\ Y_i \\ Z_i \end{bmatrix}$$

Appendix E

MATLAB® Code for Computing New Scene Illuminant

The following MATLAB® routine can be used to compute the new scene illuminant $\underset{\sim}{I}^{\lambda}$ in Section 4.4.2. In this routine, the original illuminant is assumed to be daylight $D65$. The new illuminant is assumed to be incadescent light A .

The basis functions for illuminant are provided the paper from Judd *et al.* [24]. The basis functions for reflectance are provided in the paper from Parkkinen *et al.* [36].

```
%%%%%%%%%%%%%%%%%%%%%%%%%%%%%%%%%%%%%%%%%%%%%%%%%%%%
%%%%% Compute New Scene Illuminant %%%%%%%%%%%%
%%%%%%%%%%%%%%%%%%%%%%%%%%%%%%%%%%%%%%%%%%%%%%%%%%%%

% Wavelength is taken from 400nm to 700nm, at 10nm inverval
lambda = daylight_basis_ChengLin(3:33,1); %400-700nm

% Read in the basis for daylight illuminant
I1 = daylight_basis_ChengLin(3:33,2);
```

```
I2 = daylight_basis_ChengLin(3:33,3);
I3 = daylight_basis_ChengLin(3:33,4);

% Read in the basis for reflectance
R1 = reflectance_basis_Parkkinen(1:31,2);
R2 = reflectance_basis_Parkkinen(1:31,3);
R3 = reflectance_basis_Parkkinen(1:31,4);
R_basis = [R1 R2 R3];

% Read in CIE color matching functions, 10 degree observer
x_hat = color_matching_1964_10deg (5:35, 2);
y_hat = color_matching_1964_10deg (5:35, 3);
z_hat = color_matching_1964_10deg (5:35, 4);

% Decompose original scene illuminant. The scalars are from Cheng & Lin
m = [1;-0.343;-0.664];

I = m(1,1)*I1+m(2,1)*I2+m(3,1)*I3;

% Find chromaticities of the old illuminant estimated with basis
x_I_estimate = dot(x_hat,I)/(dot(x_hat,I)+dot(y_hat,I)+dot(z_hat,I));
y_I_estimate = dot(y_hat,I)/(dot(x_hat,I)+dot(y_hat,I)+dot(z_hat,I));

% Decompose reflectance
x_est(1,1) = 0;
y_est(1,1) = 0;
x_tilda(1,1) = 0;
y_tilda(1,1) = 0;
```

```
% Read from Munsell reflectance data at 10nm interval
for i=0:30,
    munsell_10nm(i+1,:) = munsell(2*i+1,: );
end

% for j=2:25, <= uncomment this for testing Macbeth checker pattern
for j=1:1250,
    % R = reflectance_macbeth_10nm(1:31,j); <= uncomment this for testing
    % Macbeth checker pattern
    R = munsell_10nm(1:31,j);
    N = (R_basis\R)';

    x = dot(x_hat,R)/(dot(x_hat,R)+dot(y_hat,R)+dot(z_hat,R));
    y = dot(y_hat,R)/(dot(x_hat,R)+dot(y_hat,R)+dot(z_hat,R));

    R_estimate = R_basis*N';

    x_estimate = dot(x_hat,R_estimate)/(dot(x_hat,R_estimate)
                 +dot(y_hat,R_estimate)+dot(z_hat,R_estimate));
    y_estimate = dot(y_hat,R_estimate)/(dot(x_hat,R_estimate)
                 +dot(y_hat,R_estimate)+dot(z_hat,R_estimate));

    % Find chromaticities of the reflectance estimated with basis
    x_est(j,1) = x_estimate;
    y_est(j,1) = y_estimate;

    %%%%%%%%%%%%%%%%%%%%%%%%%%%%%%%%%%%
    %%%%%% Main computation %%%%%%%%%%%%
    %%%%%%%%%%%%%%%%%%%%%%%%%%%%%%%%%%%
```

```
%alpha => von Kries, M =>cone response
alpha = [100.0/110.0 0 0; 0 100.0/100.0 0; 0 0 100.0/34.0];
alpha_inv = inv(alpha);
M = [0.4 0.708 -0.081; -0.226 1.165 0.046; 0 0 0.918];
M_inv = inv(M);

%Q = IR
%LHS = BxNRI

Q11 = prod([R1'; I1'])';
Q12 = prod([R1'; I2'])';
Q13 = prod([R1'; I3'])';
Q21 = prod([R2'; I1'])';
Q22 = prod([R2'; I2'])';
Q23 = prod([R2'; I3'])';
Q31 = prod([R3'; I1'])';
Q32 = prod([R3'; I2'])';
Q33 = prod([R3'; I3'])';

%NQ (1x3) = N(1x3)*Q(3x3)
NQ11 = N(1,1)*Q11 + N(1,2)*Q21 + N(1,3)*Q31;
NQ12 = N(1,1)*Q12 + N(1,2)*Q22 + N(1,3)*Q32;
NQ13 = N(1,1)*Q13 + N(1,2)*Q23 + N(1,3)*Q33;

%A(3X3) = x(3x"1")*NQ ("1"x3)
A11 = sum(prod([x_hat'; NQ11'])');
A12 = sum(prod([x_hat'; NQ12'])');
A13 = sum(prod([x_hat'; NQ13'])');
```

```
A21 = sum(prod([y_hat'; NQ11']))';
A22 = sum(prod([y_hat'; NQ12']))';
A23 = sum(prod([y_hat'; NQ13']))';
A31 = sum(prod([z_hat'; NQ11']))';
A32 = sum(prod([z_hat'; NQ12']))';
A33 = sum(prod([z_hat'; NQ13']))';


A = [A11 A12 A13; A21 A22 A23; A31 A32 A33];

A_inv = inv(A);

B = A_inv*M_inv*alpha_inv*M*A;

m_tilda = B*m;


% Find new illuminant I_tilda
I_tilda = m_tilda(1,1)*I1+m_tilda(2,1)*I2+m_tilda(3,1)*I3;

x_I_tilda = dot(x_hat,I_tilda)/(dot(x_hat,I_tilda)
            +dot(y_hat,I_tilda)+dot(z_hat,I_tilda));
y_I_tilda = dot(y_hat,I_tilda)/(dot(x_hat,I_tilda)
            +dot(y_hat,I_tilda)+dot(z_hat,I_tilda));

x_tilda(j,1) = x_I_tilda;
y_tilda(j,1) = y_I_tilda;

% LHS with real reflectance and estimated reflectance
```

```
    I_tilda_R = prod([I_tilda'; R'])';

    x_out = dot(x_hat,I_tilda_R)/(dot(x_hat,I_tilda_R)+dot(y_hat,
            I_tilda_R)+dot(z_hat,I_tilda_R));
    y_out = dot(y_hat,I_tilda_R)/(dot(x_hat,I_tilda_R)+dot(y_hat,
            I_tilda_R)+dot(z_hat,I_tilda_R));

    I_tilda_R_estimate = prod([I_tilda'; R_estimate'])';

    x_out_estimate = dot(x_hat,I_tilda_R_estimate)/(dot(x_hat,
                     I_tilda_R_estimate)+dot(y_hat,I_tilda_R_estimate)
                     +dot(z_hat,I_tilda_R_estimate));
    y_out_estimate = dot(y_hat,I_tilda_R_estimate)/(dot(x_hat,
                     I_tilda_R_estimate)+dot(y_hat,I_tilda_R_estimate)
                     +dot(z_hat,I_tilda_R_estimate));

    % RHS with real reflectance and estimated reflectance
    I_R = prod([I'; R'])';
    x_in = dot(x_hat,I_R)/(dot(x_hat,I_R)+dot(y_hat,I_R)+dot(z_hat,I_R));
    y_in = dot(y_hat,I_R)/(dot(x_hat,I_R)+dot(y_hat,I_R)+dot(z_hat,I_R));

    I_R_estimate = prod([I'; R_estimate'])';
    x_in_estimate = dot(x_hat,I_R_estimate)/(dot(x_hat,I_R_estimate)
                    +dot(y_hat,I_R_estimate)+dot(z_hat,I_R_estimate));
    y_in_estimate = dot(y_hat,I_R_estimate)/(dot(x_hat,I_R_estimate)
                    +dot(y_hat,I_R_estimate)+dot(z_hat,I_R_estimate));

end
```

Bibliography

[1] Ambient Light Sensor (ALS) applications in portable electronics. White paper, ROHM Semiconductor, 2009. Available online. 15

[2] Vivek Agarwal, Besma R. Abidi, Adreas Koschan, and Mongi A. Abidi. An overview of color constancy algorithms. *Journal of Pattern Recognition Research*, 1:42–54, 2006. 1, 15

[3] Kobus Barnard. Color constancy with fluorescent surfaces. In *The Seventh Color Imaging Conference: Color Science, Systems, and Applications*, pages 114–119. IS&T - The Society for Imaging Science and Technology, November 1999. 15

[4] Kobus Barnard, Vlad Cardei, and Brian Funt. A comparison of computational color constancy algorithms. I: Methodology and experiments with synthesized data. *IEEE Transactions on Image Processing*, 11(9):972–984, September 2002. 15

[5] Kobus Barnard, Vlad Cardei, and Brian Funt. A comparison of computational color constancy algorithms. II: Experiments with image data. *IEEE Transactions on Image Processing*, 11(9):985–996, September 2002. 15

[6] Karen M. Braun and Mark D. Fairchild. Testing five color-appearance models for changes in viewing conditions. *Color Research & Application*, 22(3):165–173, June 1997. 12, 44

[7] Edwin J. Breneman. Corresponding chromaticities for different states of adaptation to complex visual fields. *Journal of the Optical Society of America A*, 4(6):1115–1129, 1987. 44

[8] Jozef Cohen. Dependency of the spectral reflectance curves of the Munsell color chips. *Psychonomic Science*, 1:369, 1964. 36

[9] William B. Cowan. *Handbook of Optics Volume III Vision and Vision Optics*, chapter 22: Displays for Vision Research. The McGraw-Hill Companies, 2010. 30

[10] Marc Ebner. *Color Constancy*, chapter 6: Algorithms for Color Constancy Under Uniform Illumination, pages 103–141. Wiley-IS&T Series in Imaging Science and Technology, Chichester, England, 2007. 1, 15

[11] Mark D. Fairchild. RLAB: A color appearance space for color reproduction. In *Devide-Independent Color Imaging and Imaging Systems Integration (Proceedings of SPIE)*, volume 1909, pages 19–30, San Jose, California, USA, August 1993. 12

[12] Mark D. Fairchild. *Color Appearance Models*, chapter 9, pages 211–214. Wiley-IS&T, Chichester, UK, 2005. 12, 32

[13] Mark D. Fairchild. *Color Appearance Models*, chapter 9, pages 197–214. Wiley-IS&T, Chichester, UK, 2005. 31, 44

[14] Hany Farid and Edward H. Adelson. Separating reflections and lighting using independent components analysis. In *Proceedings of the 1999 IEEE Computer Scociety Conference on Computer Vision and Pattern Recognition*, volume 1, pages 1262–1268, Colorado, USA, June 1999. 26, 56

[15] Graham D. Finlayson. Color in perspective. *IEEE Transactions on Pattern Analysis and Machine Intelligence*, 18:1034–1038, 1996. 14

[16] David A. Forsyth. A novel algorithm for color constancy. *International Journal of Computer Vision*, 5:5–36, September 1990. 1, 14

[17] William T. Freeman and David H. Brainard. Bayesian decision theory, the maximum local mass estimate, and color constancy. In *Proceedings of the Fifth International Conference on*

Computer Vision, ICCV '95, pages 210–217, Washington, DC, USA, 1995. IEEE Computer Society. 15

[18] Brian Funt and Vlad C. Cardei. Bootstrapping color constancy. In *Proceedings of SPIE: Electronic Imaging IV*, volume 3644, Denvor, CO, USA, July 1999. 15

[19] Brian V. Funt, Kobus Barnard, and Lindsay Martin. Is machine colour constancy good enough? In *Proceedings of the Fifth European Conference on Computer Vision*, volume 1 of *ECCV '98*, pages 445–459, London, UK, 1998. Springer-Verlag. 14

[20] Ron Gershon, Allan D. Jepson, and John K. Tsotsos. From [R,G,B] to surface reflectance: Computing color constant descriptors in images. In *Proceedings of the Tenth International Joint Conference on Artificial Intelligence*, volume 2, pages 755–758, San Francisco, CA, USA, 1987. Morgan Kaufmann Publishers Inc. 14

[21] Robert W.G. Hunt. A model of colour vision for predicting colour appearance in various viewing conditions. *Color Research & Application*, 12(6):297–314, 1987. 12

[22] Aapo Hyvärinen and Erkki Oja. Independent component analysis: Algorithms and applications. *Neural Networks*, 13(4-5):411–430, May 2000. 26

[23] Garrett M. Johnson and Mark D. Fairchild. Full-spectral color calculations in realistic image synthesis. *Computer Graphics and Applications, IEEE*, 19(4):47–53, July 1999. 1, 9, 11, 13

[24] Deane B. Judd, David L. Macadam, Gütnter Wyszecki, H.W.Budde, H.R.Condit, S.T. Henderson, and J.L. Simonds. Spectral distribution of typical daylight as a function of correlated color temperature. *Journal of the Optical Society of America*, 54(8):1031–1036, 1964. 36, 83

[25] Naoya Katoh, Kiyotaka Nakabayashi, Masahiko Ito, and Shin Ohno. Effect of ambient light on the color appearance of softcopy images: Mixed chromatic adaptation for self-luminous displays. *Journal of Electronic Imaging*, 7(4):794–806, January 1998. 16

[26] Bong-Soo Kim, In-Ho Song, Eun-Su Kim, Sung-Hak Lee, Soo-Wook Jang, and Kyu-Ik Sohng. Chromatic adaptation model using the relationship between the cone responses under change in illuminants. *IEICE Transactions on Fundamental Electronics, Communications and Computer Sciences*, E89-A:1717–1719, June 2006. 13

[27] Charles Kittel. *Introduction to Solid State Physics*, chapter 17:Optical Phenomena in Insulators, pages 554–556. John Wiley & Sons, Inc., New York, United States, 1966. 9

[28] Eung-Joo Lee, In-Gab Jeong, Yang-Woo Park, Yeong-Ho Ha, and Gwang-Choon Lee. Color enhancement of TV picture using RGB sensor. *IEEE Transactions on Consumer Electronics*, 42(2):182–191, May 1996. 15, 16

[29] Sung-Hak Lee, In-Ho Song, and Kyu-Ik Sohng. Color reproduction model for varying illumination conditions. *The Institute of Electronics, Information and Communication Engineers (IEICE) Transactions*, 90-C(11):2119–2125, 2007. 14

[30] M. Ronnier Luo, Anthony A. Clarke, Peter A. Rhodes, Andre Schappo, Stephen A. R. Scrivener, and Chris J. Tait. Quantifying colour appearance. Part I. LUTCHI colour appearance data. *Color Research & Application*, 16(3):166–180, June 1991. 13

[31] Jeffrey J. McConnell. *Computer Graphcis: Theory into Practice*, chapter 2: Vision, Light, and Shading, pages 49–112. Jones and Bartlett Publishers, Sudbury, MA, United States, 2006. 7

[32] Nathan Moroney, Mark D. Fairchild, Robert W. G. Hunt, Changjun Li, Ronnier M. Ronnier Luo, and Todd Newman. The CIECAM02 color appearance model. In *The Tenth Color Imaging Conference: Color Science and Engineering Systems, Technologies, Applications*, pages 23–27, Arizona, USA, November 2002. IS&T - The Society for Imaging Science and Technology. 13, 31

[33] Georg E. Müller. Über die farbenempfindungen. *Zeischrift fur Psychologie*, 17–18(46):508, 1930. 11

[34] Y. Nayatani, K. Takahama, and H. Sobagaki. Prediction of color appearance under various adapting conditions. *Color Research & Application*, 11(1):62–71, 1986. 12

[35] YungKyung Park, ChangJun Li, M. Ronnier Luo, Youngshin Kwak, Du-Sik Park, and Changyeong Kim. Applying CIECAM02 for mobile display viewing conditions. In *IS&T/SID* 15^{th} *Color Imaging Conference*, pages 169–173, Albuquerque, New Mexico, 2007. 16

[36] J. P. S. Parkkinen, J. Hallikainen, and T. Jaaskelainen. Characteristic spectra of Munsell colors. *Journal of the Optical Society of America*, 6(2):318–322, February 1989. 83

[37] Javier Romero, Antonio García-Beltrán, and Javier Hernández-Andrés. Linear bases for representation of natural and artificial illuminants. *Journal of the Optical Society of America A*, 14(5):1007–1014, 1997. 36

[38] A. Kimball Romney and Tarow Indow. Munsell reflectance spectra represented in three-dimentional Euclidean space. *Color Research & Application*, 28(3):182–196, June 2003. 36

[39] Jin-Keun Seok, Sung-Hak Lee, In-Ho Song, and Kyu-Ik Sohng. A chromatic adaptation model for mixed adaptation conditions. In *Proceedings of the 2008 International Conference on Image Processing, Computer Vision, & Pattern Recognition, IPCV*, pages 670–673, Las Vegas, Nevada, USA, July 2008. CSREA Press. 16

[40] E. I. Stearns. *Colorimetry,* 2^{nd} *Ed*. Number 15.2. Commission Internationale de L'Eclairage, Central Bureau of the CIE, Paris, 1986. 12

[41] Yinlong Sun. *A Spectrum-based Framework for Realistic Image Synthesis*. Ph.D. Thesis, Simon Fraser University, Vancouver, BC, Canada, July 2000. 1, 9, 11

[42] Steve Upstill. *The RenderMan Companion: A Programmer's Guide to Realistic Computer Graphics*. Addison-Wesley Reading, Massachusetts, United States, 1990. 7